Chemical and isotope composition of the oilfield brines from Mishrif Formation (southern Iraq): Diagenesis and geothermometry

Elsevier Editorial System(tm) for Marine and Petroleum Geology

Manuscript Draft

Manuscript Number: JMPG-D-19-01563R4

Title: Chemical and isotope composition of the oilfield brines from Mishrif Formation (southern Iraq): Diagenesis and geothermometry

Article Type: Full Length Article

Keywords: Oilfield waters; chemical composition; geothermometry; oxygen and hydrogen stable isotope ratios; strontium isotopes.

Corresponding Author: Dr. Zaher Mundher Yaseen, P.h.D

Corresponding Author's Institution: Ton Duc Thang University

First Author: Tiziano Boschetti

Order of Authors: Tiziano Boschetti; Salih Muhammad Awadh; Heba Sadoon Al-Mimar; Paola Iacumin; Lorenzo Toscani; Enricomaria Selmo; Zaher Mundher Yaseen, P.h.D

Abstract: This paper focuses on the geochemical composition and isotope geochemistry of brines in the Cenomanian-Turonian carbonate Mishrif reservoir of southern Iraq. Main dissolved constituents, trace elements, □2H and □18O, 87Sr/86Sr, mineral saturation indices and thermodynamic calculations were investigated in formation waters from the Mishrif Formation to obtain a better understanding of brine evolution and diagenetic effects over geological time. Previous published δ11B data were also reinterpreted as a geothermometer tool. The results are compared with previous published data for local oilfields and coeval formations in the Arabian Gulf. The Mishrif brine has a marine origin and is diagenetically modified to Ca-excess and Na-deficit. Formation waters are quartz supersaturated and are in equilibrium with chalcedony and calcite-dolomite in the temperatures range of 50-75°C, which is also confirmed by calcite-water oxygen isotope fractionation and δ11B geothermometer. The potential role of clays in conditioning brine chemistry during diagenetic processes was highlighted by activity diagrams; in particular, their adsorption/exchange effect on sodium could explain the lower temperature obtained by the Na/Li geothermometer (42 ± 6 °C). The □2H and □18O values show that oxygen isotope composition of the brines was isotopically more affected by interaction with limestone during diagenesis than seawater evaporation. The main effect is an 18O-enrichment on the brine starting from the SMOW value. Locally, dilution by present-day meteoric water was also detected (Rumaila South), which is shifted towards the local meteoric water line. The strontium isotope ratios range from 0.707713 to 0.707749 and correspond to a marine strontium of late Cenomanian-early Maastrichtian age, except for the Majnoon sample, which shows a more radiogenic value (0.708043). Radiogenic strontium and gypsum and anhydrite saturation indices of the Majnoon sample could indicate the contribution of calcium and sulphate from the strontium-rich sulphate minerals of the Cambrian salt domes occurring in the oilfields of southern Iraq. The higher manganese concentration (4 mg/l) and the slightly higher temperature inferred by geothermometers (up to 74 °C) in comparison with present-day could

indicate that the Majnoon brine is a hot fluid, probably related to a deeper structure such as the Zagros Foredeep Fault.

Research Data Related to this Submission

There are no linked research data sets for this submission. The following reason is given:
The used data has been reported in the manuscript.

Chemical and isotope composition of the oilfield brines from Mishrif Formation (southern Iraq): Diagenesis and geothermometry

The authors very much appreciate the respected Editor for his constructive revision and all the technical and grammatical corrections.

IMPORTANT NOTE: Reviewer attachments may have been uploaded to EES. If there are attachments for your paper, you can view them by clicking on the View Reviewer Attachments action link in EES.

Reviewers' comments:

Associate Editor Katz's comments:

* Please review the highlighted wording, grammar and style revisions and make the appropriate revisions.

- All the reported language edits have been revised and modified accordingly.

Highlights

- Sr, O and H isotopic composition of formation brine from southern Iraq are presented
- Calcite-dolomite and chalcedony equilibria with water were achieved during diagenesis
- Chemically inferred and calcite-water oxygen isotope fractionation temperature agree
- Mineralogical composition is confirmed by plotting water samples on activity diagram

Chemical and isotope composition of the oilfield brines from Mishrif Formation (southern Iraq): Diagenesis and geothermometry

Tiziano Boschetti[1], Salih Muhammad Awadh[2], Heba Sadoon Al-Mimar[2], Paola Iacumin[1], Lorenzo Toscani[1], Enricomaria Selmo[1], Zaher Mundher Yaseen[3,*]

[1] Department of Chemistry, Life Sciences and Environmental Sustainability, University of Parma, Parco Area delle Scienze 157/A, 43124 Parma, Italy

[2] Department of Geology, College of Science, University of Baghdad, Baghdad, Iraq

[3] Sustainable Developments in Civil Engineering Research Group, Faculty of Civil Engineering, Ton Duc Thang University, Ho Chi Minh City, Vietnam

*Corresponding authors: Zaher Mundher Yaseen

Email: yaseen@tdtu.edu.vn

Abstract

This paper focuses on the geochemical composition and isotope geochemistry of brines in the Cenomanian–Turonian carbonate Mishrif reservoir of southern Iraq. Main dissolved constituents, trace elements, $\delta^{2}H$ and $\delta^{18}O$, $^{87}Sr/^{86}Sr$, mineral saturation indices and thermodynamic calculations were investigated in formation waters from the Mishrif Formation to obtain a better understanding of brine evolution and diagenetic effects over geological time. Previous published $\delta^{11}B$ data were also reinterpreted as a geothermometer tool. The results are compared with previous published data for local oilfields and coeval formations in the Arabian Gulf. The Mishrif brine has a marine origin and is diagenetically modified to Ca-excess and Na-deficit. Formation waters are quartz supersaturated and are in equilibrium with chalcedony and calcite-dolomite in the temperatures range of 50–75°C, which is also confirmed by calcite-water oxygen isotope fractionation and $\delta^{11}B$ geothermometer. The potential role of clays in conditioning brine chemistry during diagenetic processes was highlighted by activity diagrams; in particular, their adsorption/exchange effect on sodium could explain the lower temperature obtained by the Na/Li geothermometer (42 ± 6 °C). The $\delta^{2}H$ and $\delta^{18}O$ values show that oxygen isotope composition of the brines was isotopically more affected by interaction with limestone during diagenesis than seawater evaporation. The main effect is an ^{18}O-enrichment on the brine starting from the SMOW value. Locally, dilution by present-day meteoric water was also detected (Rumaila South), which is shifted towards the local meteoric water line. The strontium isotope ratios range from 0.707713 to 0.707749 and correspond to a marine strontium of late Cenomanian–early Maastrichtian age, except for the Majnoon sample, which shows a more radiogenic value (0.708043). Radiogenic strontium and gypsum and anhydrite saturation indices of the Majnoon sample could indicate the contribution of calcium and sulphate from the strontium-rich sulphate minerals of the Cambrian salt domes occurring in the oilfields of southern Iraq.

The higher manganese concentration (4 mg/l) and the slightly higher temperature inferred by geothermometers (up to 74 °C) in comparison with present-day could indicate that the Majnoon brine is a hot fluid, probably related to a deeper structure such as the Zagros Foredeep Fault.

Keywords: Oilfield waters; chemical composition; geothermometry; oxygen and hydrogen stable isotope ratios; strontium isotopes.

1. Introduction

In the Jurassic–Cretaceous petroleum system of southern Iraq, hydrocarbons are mainly trapped in Lower Cretaceous sandstone and carbonate reservoirs. Crude oil is generated from the organic-rich Upper Jurassic (Sargelu and Sulaiy formations) changing the Lower Cretaceous carbonates of the Yamama Formation and the Zubair Formation, a clastics reservoir (Abeed et al., 2012; Abeed et al., 2013). The chemical composition of formation waters from the Yamama reservoir in the Zubair and North/South Rumaila oilfields is mainly composed of chloride (up to 143,589 ppm) with a salinity 6.2 times higher than seawater (Jamil, 1978), as for West Qurna oilfield, salinity 7.3 times higher than seawater and dominated by 191,700 ppm of chloride (Al-Marsoumi and Abdul-Wahab, 2005). These prior works utilized brine chemistry but did not address the evolution of the reservoir brine, as they relied mainly on cations and anions without considering isotopes. More recently, the boron stable isotope ratio of the brine from the Mishrif reservoir has given a seawater signature (Awadh et al., 2019a; Awadh et al., 2018) and highlighted the role of salinity in generating the formation pressure and controlling the fluid flow (Al-Mimar and Awadh, 2019). The developing of the oilfield brines over the geological time and its response to the flooding and diagenesis have a significant impact on petroleum reservoir quality, but this subject has not yet been investigated.

The diagenetic effects on brine waters can be evaluated by comparing the Na, Ca and Cl concentrations of the brine with those of seawater and with the so-called basinal fluid line in the Ca-excess versus Na-deficit binary diagram (Davisson and Criss, 1996). However, in this plot the interpretation could be misguided because: (i) the reference basinal fluid line takes into account only plagioclase albitisation, often without checking the real thermodynamic equilibria state of the involved waters; and ii) modelling involves the current seawater composition disregarding that of past periods (Bąbel and Schreiber, 2014; Lowenstein et al., 2003). A combination of isotope parameters as O-H stable isotope ratios and $^{87}Sr/^{86}Sr$ was proposed by Danquigny et al. (2005) to evaluate the effect of water flooding in the Mishrif Formation water of Qatar. However, in that work, seawater evaporation, the isotope salt effect (Horita et al., 1993), and the contribution of radiogenic strontium to the limestones of the Mishrif Formation were not considered.

The objectives of this research are: i) to investigate the origin of the oilfield waters; ii) to evaluate the composition of oilfield waters over time; and iii) to trace the influence of diagenesis and any geothermal effects on the brine. This investigation considers the above described effects and processes in the Mishrif Formation brines by reinterpreting the previously published main chemical constituents, along with new and original data on trace elements, oxygen and hydrogen water isotope ratio, the $^{87}Sr/^{86}Sr$ ratio, and thermodynamic calculations. Moreover, the previously published data of boron isotope ratio $\delta^{11}B$ (Awadh et al., 2019a; Awadh et al., 2018) are here reinterpreted as a geothermometer tool, and are results compared with those obtained from chemical geothermometers. The main research contribution is to obtain better understanding of the oilfield brines evolution.

2. Geological setting

2.1. Oilfield locations, main geological features and tectonics

The studied oilfields, Rumaila South (RU), Rumaila North (R), West Qurna (WQ), Zubair (ZB) and Majnoon (MJ) are located in southern part of Iraq (Jassim and Buday, 2006) (Fig. 1A). The Mesopotamian zone extends from middle to southern Iraq as a relatively flat terrain with a gradient of less than 10 cm/km in the north-west to the Arabian Gulf. The zone was probably uplifted during Hercynian deformation but was subject to subsidence from the Late Permian onwards (Jassim and Buday, 2006). The oilfields are located in the Zubair zone (Grabowski Jr., 2014; Sadooni and Aqrawi, 2000), southern part of the Mesopotamia plain (Fig. 1A), an area characterized by the presence of a gentle subsurface succession of anticlinal and synclinal structures. These structures form giant hydrocarbon traps: Rumaila South (37 km length, 16 km width), Rumaila North (40 km, 13.5 km), West Qurna (35 km, 8 km) and Majnoon (48 km, 10 km).

From the interpretation of gravity and magnetic data, Alyasi et al. (2014) mentioned that the presence of anticlinal structures is due to the effect of the evaporites of the Late Jurassic Gotnia Formation and Late Ediacaran – Early Cambrian Hormuz Formation in addition to other tectonic forces, where salts moves upward by buoyant forces and the denser rocks remain below them. To the north of the Arabian Gulf, huge salt-gypsum domes are exposed at a surface coexisting with a mixture of igneous and metamorphic rocks peeled off from the Precambrian crystalline basement (Mortazavi et al., 2017). Jabal Sanam is one of the salt diapirs in southern Iraq / northern Kuwait border (Fig. 1); it is an extension of the Hormuz Formation, located in Iran at the northern part of the Arabian Gulf, which contains more than 200 salt domes composed of sequences of evaporates, shales, siltstones and carbonates (Mortazavi et al., 2017). The role of tectonic events (extensional faulting) and differential loading of sedimentary cover above the mobile salt layer are the main triggering factors of the salt diapirism (Singh, 2012). In particular, the Permo-Triassic Tethyan rifting, the Cretaceous-Paleogene obduction and the compressive events associated with basement

reactivation of north-south Arabian trends could have started the episodic salt diapir activity in the area of this study (Singh, 2012). However, traces of a neotectonic reactivation were also documented (Sissakian et al., 2017).

The Zubair zone is a southern part of the Mesopotamian Basin that is located close to the junction of the Arabian Shelf and Iranian continental block. Collision of these plates at the Mesozoic-Cenozoic boundary produced the Zagros Foredeep fault and the Mesopotamian Basin, which is a member of the Arabian Gulf Basin (Konyuhov and Maleki, 2006). During the Mesozoic and Cenozoic, the study area was a tropical region, with organic-rich carbonates or organic-rich argillaceous sediments being deposited. Good-quality source rocks were preserved in different intervals of geological time, particularly during the Mesozoic. For example (Fig. 1B): the Alan Formation in the Middle Jurassic; the Sargelu, Najmah and Sulaiy formations are the source rocks in the Upper Jurassic; the Yamama Formation is a reservoir and productive carbonate and the Zubair Formation is a reservoir and productive sand in the Lower Cretaceous; the Ratawi, Shuaiba and Nahr Umr formations are carbonate reservoirs in the Lower Cretaceous. The Mauddud, Ahmadi and Rumaila formations are the mainly carbonate reservoirs in the Cenomanian. The Mishrif Formation is a main carbonate reservoir of the Cenomainan-Touronian (Fig. 1B). The Khasib and Tanuma formations are poor reservoirs. Tectonic fracturing of younger higher carbonate permits vertical migration of hydrocarbons into anticlines under efficient evaporitic seals. The regional evaporite seal is Gotnia Formation in the Upper Jurassic, and Fat'ha Formation in the Tertiary (Fig. 1B).

2.2. Stratigraphy, paleogeography and mineralogy

The Mishrif Formation is the main productive reservoir in southern Iraq, the United Arab Emirates, Oman, and Qatar. It was deposited in a shallow environment on the Rumaila Formation conformity. Its upper contact is unconformable with the Khasib Formation, representing a regression in the Turonian-Campanian age (Al-Mimar et al., 2018;

Awadeesian et al., 2019). It is represented by a unique lithostratigraphic unit regionally deposited in a fluctuating environment of shallow to deep-water reflecting the tectonic activity in the area (Alsharhan and Nairn, 1988). The carbonate rocks are composed of bioclastic particles (algae, rudist and coral reef) and represent the main facies of the Mishrif Formation. In terms of mineralogy, the Mishrif Formation is mainly composed of calcite (90% av.), with heterogeneous distribution of small amounts of dolomite, kaolinite, chlorite, authigenic quartz and clays (smectites and mixed layers) that do not exceed 10% (Al-Mimar et al., 2018). Southwardly, facies change to distal mid-ramp and proximal mid-ramp deposits and grade into outer-ramp deposits (Aqrawi et al., 1998). Eastwardly, close to the Zagros Foredeep Fault (ZFF) on the border with Iran, the Mishrif Formation is thicker (up to 400 m) and deeper (up to 3000 m) (Abbas and Mahdi, 2019; Mahdi et al., 2013). In particular, thick lagoonal units were deposited in the Majnoon field, implying a paleogeographic change in the eastern part of the study area where carbonate production caught up with the rising sea level until the filling of accommodation space with lagoonal deposits (Mahdi et al., 2013). The movement of the Hormuz Formation's salts was particularly important in southern Iraq (Murris, 1980). Sadooni (2005) suggested that rudist build-ups in the Baṣrah area nucleated on the crests of growing salt structures. When the build-ups reached wave-base, they were eroded and rudist fragments were reworked, transported and dispersed to form bioclastic packstone/grainstones (Aqrawi et al., 2010).

3. Methodology

3.1. Chemical and isotope analyses

Physicochemical parameters and major ion composition of five formation water samples from Rumaila South (RU287), Rumaila North (R590), West Qurna (WQ87), Majnoon (MJ20), and Zubair (ZB140) oilfields were reprised from Awadh et al. (2018) (mean values

and standard deviations at N = 28) and reinterpreted to investigate diagenesis and the temperature of the system using geothermometry. In this study, trace elements (total sulphur, Ba, Li, Fe, Mn, Rb, Sr) were analysed at the ALS Group Laboratory in Seville (Spain) using Inductively Coupled Plasma-Atomic Emission Spectroscopy (ICP-AES; ALS analytical code ME-ICP14L) after filtration and acidification by nitric acid. The dissolved silica as $SiO_2(aq)$ was analysed using the heteropoly blue spectrophotometric method (Clesceri et al., 1999) on filtered and diluted (1:5 by 18 MOhm ASTM Type 1 water) samples. The delta isotope values of hydrogen and oxygen of water molecules in ‰ versus V-SMOW reference standard $\delta^2H(H_2O)_c$ and $\delta^{18}O(H_2O)_c$, respectively, were obtained; where subscript 'c' represents the 'composition' scale (Horita et al., 1993). These isotope measurements were conducted by the H_2-H_2O and CO_2-H_2O gas equilibration isotope ratio mass spectrometry (IRMS) method on the vacuum-distilled samples (Boschetti et al., 2011). The salt effect parameter $10^3 ln\Gamma$ of the brines was calculated taking into account the chemical composition and the temperature of the samples by PHREEQCI code, version 3, with the Pitzer thermodynamic database (Boschetti et al., 2011; Horita et al., 1993; Parkhurst and Appelo, 2013). According to Horita et al. (1993), the delta activity of hydrogen and oxygen, $\delta^2H(H_2O)_a$ and $\delta^{18}O(H_2O)_a$, respectively, was obtained summing the salt effect parameter and the delta isotope composition of hydrogen and oxygen.

The strontium isotope ratios, $^{87}Sr/^{86}Sr$, of the brines were obtained using thermal ionization mass spectrometry (TIMS). Prior to the analytical process, separation of Sr from the matrix bulk elements, and especially from Rb, was executed using heat plate evaporation with Teflon® vials at 80°C, followed by chromatographic extraction using Sr-Resin™ (TrisKem International) (crown-ether (4, 4' (5')-di-t-butylcyclohexano-18-crown-6). The final Sr fraction was recovered from the bulk using HNO_3 0.05M as eluent, then evaporated on a heat plate at 80°C and introduced into the mass spectrometer. Possible ^{87}Rb interferences

were corrected in the Sr analysis and the $^{87}Sr/^{86}Sr$ ratio was normalised in order to correct for mass fractionation, taking into account a reference value of $^{86}Sr/^{88}Sr = 0.1194$. The $^{87}Sr/^{86}Sr$ results were normalised to NBS SRM 987 (National Bureau of Standards Standard Reference Material 987 – strontium carbonate). Internal precision was 3×10^{-6}.

3.2. Thermodynamic calculations

PHREEQCI code and Pitzer thermodynamic dataset were also used to define:

i) the mineral-water saturation indices SI = log(IAP/K), where IAP and K are the ion activity product of the dissolved constituents and K is the mineral solubility product in a specific reaction, respectively, and the partial pressure of carbon dioxide by the Peng–Robinson equation of state (Parkhurst and Appelo, 2013);

ii) a geothermal model based on multimineral equilibria.

Results were compared to previously published chemical and isotopic geothermometers specific for sedimentary brines (Boschetti et al., 2015; Kharaka and Mariner, 1989; Sanjuan et al., 2014). The calculated activity of the dissolved constituents was also used to calculate the saturation index of a carbonate solid solution made of calcite, magnesite, rhodochrosite, siderite and strontianite by EQ3/6 code, version 8 (Wolery and Jarek, 2003).

The Geochemist's Workbench® code (GWB), version 7.0.6 (Bethke and Yeakel, 2008), was used to calculate the evaporation path of Cretaceous seawater using the React tool, HMW thermodynamic database, and the main chemical composition of seawater during that period (Bąbel and Schreiber, 2014). According to Bąbel and Schreiber (2014), a chloride concentration of present-day seawater (565 mmol kg^{-1} H_2O) was taken as a reference; then chloride concentration was charge-balanced, taking into account other main constituents and pH = 7.5 (Hönisch et al., 2012), and a $\log PCO_2(g) = -3$ was settled during evaporation. This

latter corresponded to a mean concentration of 1000 ppmv of CO_2 in the Cretaceous atmosphere (Hönisch et al., 2012; Wang et al., 2014).

Finally, activity diagrams using a thermodynamic database of the minerals and dissolved constituents, recalculated at a pressure of 20 MPa, were plotted using the Act tool of the GWB-code (Boschetti et al., 2016). The Rxn tool of the same code was also used to check the thermodynamic equilibria of specific reactions.

4. Results and Discussion

The physicochemical and isotope parameters are reported in Table 1. The recalculated main chemical composition in equivalents per liter of formation water from the southern region of Iraq shows a Cl-Na composition. In particular, the Na/Cl equivalent ratios range span between 0.77 and 0.91, with a mean of 0.83 ± 0.05, which is similar to that of present-day seawater (0.86). The Ca/(SO_4 + HCO_3) equivalent ratios of the brines are largely over 1, with a mean of 44 ± 19 and a range between 15 and 78. Therefore, brines can be classified also as Ca-Cl, according to Rosenthal (1997). The mean measured temperature of the water sampled in the Mishrif Formation is 65 ± 2 °C (N = 28) (Awadh et al., 2018). Between the investigated trace elements, the concentration of barium and manganese are higher in Majnoon (5.43 and 4.47 mg/l, respectively) in comparison with the range of the samples from the other oilfields (1.44-1.79 and 0.10-0.13 mg/l, respectively). All samples showed supersaturation in calcite, aragonite, and dolomite (Table 2). Barite and anhydrite are also supersaturated in all but one sample (RU287). Finally, waters are in equilibrium with chalcedony and oversaturated in quartz.

4.1 Chemical composition: diagenesis and geothermometry

According to the previous published works on southern Iraq oilfields (Awadh et al., 2019a; Awadh et al., 2018), the above described chemical ratios of Na/Cl = 0.83 ± 0.05 and Ca/(SO_4

+ HCO_3) = 44 ± 19 are typical of marine origin formation waters that have undergone chemical modification due to diagenesis (Boschetti et al., 2011; Rosenthal, 1997). The Langelier–Ludwig and brine differentiation diagrams (Boschetti, 2011; Hounslow, 1995) of Figure 2 depict the distinct composition of the oilfield brines in comparison with the local shallow groundwater (Hamdan, 2017) and surface waters (Al-Mallah, 2014; ROPME, 2011; Rzóska, 1980). Surface water (Ghalib and Almallah, 2017), water produced from crude oil dehydration (Al-Shamkhani, 2013) or a mixture of both were used in the oilfields for water-flooding purposes. In Figure 2A, the brine samples from this study and literature are grouped in a narrow field, whereas in the brine differentiation plot (Figure 2B), brines are displaced between the evaporation curve of Cretaceous seawater and the produced waters from dehydrators (Al-Furaiji, 2016; Al-Shamkhani, 2013). Similarly to the Cretaceous formation brines in Venezuela (Boschetti et al., 2016), most of the studied brines affected by diagenesis show a Ca-excess and Na-deficit and seem to follow the typical Ca-Na exchange trend of the so-called basinal fluid line (Davisson and Criss, 1996) (Figure 3). Sample RU287 was probably affected by dolomitization and then by mixing with waters produced from crude dehydrators ("produced water" field in Figure 3). The hottest (115°C) water sample from the deeper Zubair sandstone indicates that the chemical effects of Ca-Na reactions (Al-Marsoumi and Abdul-Wahab, 2005), most probably due to albitisation, are more pronounced at higher temperatures (Figure 3A). Different from the Mishrif Formation, albite was found in the Zubair Formation (Al-Ziayyir, 2018). Moreover, from a theoretical point of view, the diagenetic effects could be more or less pronounced if the variability of the seawater composition in the past was considered. If Cretaceous seawater is used as a reference instead of present-day seawater, the oilfield brines are more clustered towards the axes origin of Figure 3B (which coincides with the composition of less saline surface water) or towards the "produced water" fields. The dolomitization process seems to have had a greater role in the

Ca-excess of the waters (Figure 3B). However, the geothermal modelling indicated in Figure 4, also suggests that calcite-dolomite equilibration occurred along with chalcedony instead of quartz. In that diagram, all but one sample are clustered between 50 and 75°C isotherms, a range that includes the temperatures of 64 ± 5°C (N = 9) and 64 ± 7°C (N = 5) obtained by Mg-Li and chalcedony geothermometers, respectively — the latter corrected for dissolved silica activity and pressure (Kharaka and Mariner, 1989) (Table 2). The exception is represented by sample MJ20 (Majnoon oilfield), which is shifted towards the quartz-dolomite (ordered) model (Figure 4) and shows the lowest temperature from quartz and chalcedony from geothermometric equations (Table 2). Such an apparent convergence between quartz and chalcedony is probably attributable to the greater depth and pressure in the MJ20 borehole (Table 1), conditions that could enhance simultaneous equilibria between the fluid and the two mineral phases (Giggenbach, 1991). For the MJ20 sample, a mean value of 70.5°C between the geothermometric equations of quartz and chalcedony shows a good agreement with the 68°C obtained from the Mg-Li geothermometer (Table 2).

Globally, the mean inferred temperature of the brines are quite similar to the mean temperature measured at depth, confirming that the present-day borehole temperatures are not so different from those reached during Neogene burial (Abeed et al., 2013). Sample MJ20 is an exception, showing a temperature 10°C higher. This is probably due to the effect of greater borehole depth (Fig. 1B) and pressure. The Majnoon oilfield had the highest measured values (Table 1). Activity diagrams of Figures 5A and 5B show that Mg concentration in the brine seems to be limited by dolomite and by chlorite. To check the coexistence of the minerals, the thermodynamics of the following reaction have been calculated (Supplementary File 1):

$$CaMg(CO_3)_2 + 0.2\ Al_2Si_2O_5(OH)_4 + Ca^{2+} + 0.2\ SiO_2(aq) + 1.4\ H_2O =$$

$= 2\ H^+ + 0.2\ Mg_5Al_2Si_3O_{10}(OH)_8 + 2\ CaCO_3$

At P = 20 MPa and buffering conditions of Figure 5A, except for Mg which has been buffered by clinochlore, $Mg_5Al_2Si_3O_{10}(OH)_8$, instead of dolomite. The above reaction is in equilibria at 64°C using $\log[Ca^{2+}/(H^+)^2]$ = 11.11 and $\log[SiO_2(aq)]$ = -3.32, which corresponds to the mean activity values of all investigated samples (Supplementary File 1). Therefore, this corroborates not only that dolomite and chlorite could coexist in the studied basin, but also the temperature values obtained by geothermometers, in particular those by Li-Mg and chalcedony equations (Table 2).

Figure 5 also shows that the Ca/Na ratio is probably controlled by smectite instead of albite. The role of clays on the control of Na amount in solution by Ca-Na exchange or Na adsorption could also explain the lower temperatures of 42 ± 6 °C obtained using the Na/Li geothermometer (Kharaka and Mariner, 1989; Sanjuan et al., 2014) (Table 2). Similarly, the values obtained from the boron isotope geothermometer gave an underestimation of the brine temperature (Table 2). This could be due to a higher $\delta^{11}B$ value in Cretaceous seawater (up to 3‰ higher than the present; Lemarchand et al. 2002), together with a fractionation effect due to evaporation up to halite saturation (approximatively +4‰) (Vengosh et al. 1992). Actually, by subtracting a value of 7‰ from the original values of the brines, a mean temperature of 64 ± 6°C was obtained from the boron isotope geothermometric equation (Boschetti et al., 2015), which matches with that obtained by the calcite-dolomite-chlorite-kaolinite equilibria.

4.2. Oxygen and hydrogen stable isotope ratios

The isotope composition value — i.e. not considering the salt effect according to Horita et al. (1993) — of the studied formation water is similar to that of the Mishrif Formation values from the Qatar oilfield values (Danquigny et al., 2005) (Figure 6). However, the calculation of isotope activity due to the salt effect reveals a high enrichment in δ^2H (up to +8.3‰) and a

slight depletion in $\delta^{18}O$ (up to -0.3‰) in comparison to the analysed isotope composition. As presented in Figure 6, the isotope composition of the formation waters from the samples analyzed in this study fall close to the final part of the hook path derived from experimental seawater evaporation (e.g. Gonfiantini et al., 2018), thus confirming the marine origin of these samples, as previously inferred by the boron isotope (Awadh et al., 2018). It should be noted that the experimental hook paths of the evaporated seawater are generally analysed from salt pans without the addition of either new marine or meteoric water (i.e. closed system) (Gonfiantini, 1965; Gonfiantini et al., 2018). This could be the reason why the isotope activity values of the brine — i.e. considering the salt effect according to Horita et al. (1993) — do not fall on the hook path (Figure 6). In Figure 6, the Iraq meteoric water line (IMWL) and its prediction interval (parallel dashed lines with $\delta^{2}H \pm 10.3$ ‰ from IMWL) were recalculated from the rainwater isotope data of Ali et al. (2015) using the error-in-variable (EIV) regression method (Boschetti et al., 2019). The extrapolation of the best fit line of the brine samples meets the prediction interval of the meteoric water line just between rain waters collected from Baṣrah city (Fig. 1) plus other southern Iraq areas (Al-Kinani et al., 2018; Ali et al., 2015; Jassem et al., 2018) and evaporated river samples from the Tigris and Euphrates (Jassem et al., 2018) (Figure 6). Sample RU287 shows the highest contribution of modern fresh water. It should also be remarked that, in comparison with other samples, the RU287 brine displays barite supersaturation (Table 2), which is probably due to the effect of mixing between brines and local water of meteoric origin or reinjected produced waters as a consequence of the water flooding (Ghalib and Almallah, 2017; Sorbie and Mackay, 2000). This is in line with the previously described chemical diagrams. On the opposite side, the extrapolated best fit line of the isotope activity of the brines meets the hooked evaporation path of seawater just on the top of the hump (Figure 6), which approximatively corresponds to gypsum saturation (Holser, 1979; Knauth and Beeunas, 1986).

Evaporated seawater samples from present-day sabkha and lagoon environments (i.e. open systems) show $\delta^{18}O$ up to +6.5‰, which is similar to those determined in the formation brines of this study, but with $\delta^{2}H$ enrichment up to approximatively +30‰ (McKenzie et al., 1980; Nadler and Magaritz, 1980; Robinson and Gunatilaka, 1991). Lower deuterium values are mainly due to mixing with evaporated surface waters or groundwater of meteoric origin (McKenzie et al., 1980; Robinson and Gunatilaka, 1991); whereas, flooding and mixing of evaporated solution with new seawater inputs could shift the composition back to the starting values (i.e. near V-SMOW) (Nadler and Magaritz, 1980) (Figure 6). A similar effect was observed in Miocene brines by comparison with $\delta^{18}O$ from coeval gypsum, with the exception of the formation waters affected by a positive $\delta^{18}O$-shift as result of diagenetic water-rock interaction with limestones (Boschetti et al., 2011). In a similar way, and assuming that starting seawater during the Phanerozoic has remained isotopically similar to the present-day V-SMOW value (i.e. 0‰ both for oxygen and for hydrogen stable isotope ratios) (Gregory and Taylor Jr, 1981; Ryb and Eiler, 2018; Sessions, 2016), the ^{18}O enrichment of formation waters as observed in samples MJ20, ZB140, and R590 could be due to water–rock interaction. Therefore, water-rock interaction and dilution seem to be the main processes that affected in a significant manner the isotope composition of the studied brines.

Such a diagenetic effect was also hypothesised for the Mishrif Formation in Qatar where limestones value ranges between +24.4 ‰ < $\delta^{18}O$ (V-SMOW) < +27.4 ‰, formation brines $\delta^{18}O$ up to +5‰ (V-SMOW), and temperatures between 50 and 70°C have been measured (Deville de Periere, 2011). As the isotope values of the limestones from the same formation in southern Iraq are within the range of those measured in Qatar, i.e. +25.2 ‰ < $\delta^{18}O$ (V-SMOW) < +27.4 ‰ (Taha and Abdullah, 2019), the diagenetic effect can be hypothesised also for this area. Considering a mean value $\delta^{18}O(H_2O)a$ = +3.9 ‰ (V-SMOW) for the brine samples that fall within the diagenetic arrow in Figure 6 and a mean value of

$\delta^{18}O$ (limestones) equal to +26.5 ‰ (V-SMOW) of the Mishrif Formation in southern Iraq, it is possible to calculate an oxygen isotope fractionation factor of 1000lnα (calcite-water) = +22.3 ‰. This latter value corresponds to a temperature between 56°C (Kim and O'Neil, 1997) and 69°C (Zheng, 1999). Other isotope effects due to clays and crude are probably not quantitatively important or less pronounced than the salt effect. Indeed, a fractionation between water and hydrocarbons should generate in brines a shift towards $\delta^{2}H$ values higher than seawater (e.g., Horita, 2009), but this is not the case (Figure 6). Furthermore, the amount of clays minerals in the Mishrif Formation are probably insufficient to generate a significant isotope effect on the $\delta^{2}H$ of the waters.

4.3. Strontium isotope ratio

The strontium isotope ratios of the four brine samples analysed are $0.707713 < {}^{87}Sr/{}^{86}Sr < 0.707749$ (WQ87, RU287, ZB140, R590), which corresponds to a marine strontium of late Cenomanian–early Maastrichtian age (McArthur, 2010; McArthur et al., 2012); with the sample at the Majnoon oilfield (MJ20) showing the highest value of 0.708043. The Mishrif reservoir is Cenomanian–Turonian; therefore, the strontium isotope ratio should theoretically not be greater than 0.707314 ± 0.000005 (McArthur, 2010; McArthur et al., 2012). The higher strontium isotope ratios in formation waters could suggest a contribution of more radiogenic strontium from injected waters when compared to the more saline and enriched brines (Danquigny et al., 2005), but in this case the oxygen and hydrogen stable isotope ratios are not less than the other samples. Moreover, it should be also noted that ${}^{87}Sr/{}^{86}Sr$ values up to 0.707869 have been detected in the brines from the Mishrif Formation in Qatar (Al Khalij offshore field; Danquigny et al. 2005) and up to 0.70878 in the carbonate matrix of the coeval Sarvak Formation in southern Iran (Hajikazemi et al., 2012). Such elevated values detected at the disconformity surfaces of the formations are probably due to the contribution of meteoric water during diagenesis (e.g., Hajikazemi et al. 2012). However, the combination of high

manganese and radiogenic strontium contributions to the limestones of the Sarvak Formation of southern Iran were also attributed to different sources: i) a Cenomanian-Turonian subaerial exposure; ii) diagenetic fluids; and iii) detritus (Navidtalab et al., 2016). Actually, all the inspected brines of this study are undersatured with respect to pure rhodocrosite (SI = -3.9 ± 0.8), but in equilibrium with carbonate solid solution (SI = -0.082 ± 0.261) (Table 2). In particular, despite its high Mn activity, the Majnoon brine MJ20 showed a slight undersaturation in that solid solution. Therefore, the higher Mn concentration (up to 4 mg/l) and radiogenic strontium at that brine could be acquired by limestone dissolution in a disconformity layers. Alternatively, as suggested by the lowest gypsum and anhydrite saturation indices of the Majnoon sample (Table 2), it cannot be excluded that there was a contribution of radiogenic strontium-rich sulphate minerals from Cambrian salt domes (up to 0.7092) (McArthur et al., 2012). Salt domes characterise the fold settings in the oilfields of southern Iraq (Al-Ameri et al., 2011; Al-Mimar and Awadh, 2019). The doming triggered local uplift and emergence of paleo-exposure surfaces (Rahimpour-Bonab et al., 2013), thus the shallow back shoal/lagoonal depositional environment of Mishrif limestones at the Majnoon oilfield and the salt domes seem to be related (Aqrawi et al., 2010; Mahdi et al., 2013). Moreover, “hydrothermal fluids” with temperatures up to 80°C were hypothesized to form diagenetic cements (i.e., blocky calcite), dolomite and coarse crystalline pyrite during deeper burial of the Sarvak Formation (Hajikazemi et al., 2017). Therefore, the chemical, thermal and isotopic anomalies of the Majnoon brine suggest that it is the hottest fluid probably related to the higher geothermal gradient of a deeper structure as the ZFF (Basilici et al., 2020; Bordenave, 2008; Bordenave and Hegre, 2010).

5. Conclusions

This paper presented the first data on isotope ratios of oxygen, hydrogen, and strontium of oilfield waters from southern Iraq, along with new trace element data and a reinterpretation of

previous published chemistry. Processes like diagenesis and seawater evaporation that typically occur in these fluids can be distinguished using classical 'basinal fluid' chemical diagrams. Mishrif Formation waters are Cretaceous connate brines and the different chemical composition of seawater of that period needs to be taken into account for a more correct interpretation. The Ca-excess versus Na-deficit composition of these kinds of fluids are usually explained by albitisation. However, it was verified by activity plots that in the Mishrif limestone reservoir the Na/Ca exchange that occurs in brines is mainly due to water-smectite equilibrium.

The values $\delta^{2}H$ and $\delta^{18}O$ obtained on selected samples show that oxygen isotope composition of the brines was isotopically more affected by equilibria with limestone than evaporation. The global effect of the water-rock interaction is an ^{18}O-enrichment of the brines. Locally, dilution by present-day water of meteoric origin and shift towards the local meteoric water line also detected, probably as consequence of water-flooding (Rumaila South, sample RU287). Furthermore, it is also shown that isotope data cannot be separated from the interpretation of the chemical composition of sedimentary brines. The contribution of the salt effect on the stable isotope ratios of water molecules, i.e. $^{2}H/^{1}H$ and $^{18}O/^{16}O$, needs to be evaluated because this parameter could vary the results during fractionation processes such as seawater evaporation and diagenesis. Hydrogen isotope ratios are probably more affected by the salt effect than other fractionations. Furthermore, taking into account the salt effect, the temperature range inferred from carbonate-water oxygen isotope ratio fractionation is comparable to that obtained from the chemical geothermometers, i.e. between 50 and 75°C. According to Abeed et al. (2013), these evaluations confirm that the present-day borehole temperatures are not so different from those reached during Neogene burial.

More recent mixing processes such as water floods could be detected by a comparison with the composition of the formation brine, waters produced from crude dehydrators, and

the local waters of meteoric origin. The strontium isotope ratio confirms the interaction of Cretaceous limestone for most of the studied samples, suggesting a late Cenomanian–early Maastrichtian age, and an input of more radiogenic strontium in the Majnoon oilfield (MJ20 sample). The brine sample from this latter oilfield showed a particular geochemical characteristic. Despite the lower temperature measured at the MJ20 borehole (60°C), the slightly higher temperature obtained by the Li-Mg, Na-Li and $\delta^{11}B$ geothermometers (up to 74°C) is probably due to the deeper structure of that oilfield, which is closer to the ZFF. The more radiogenic strontium ratio at Majnoon could be related to: i) debris input in the limestone, which could explain also the high Mn content; or ii) interaction with local Cambrian sulphates. An inspection of additional samples, sulphur stable isotope ratio ($^{34}S/^{32}S$) and radiogenic isotope of the halogens (^{139}I, ^{36}Cl) could improve the knowledge of the past water flow events and clarify the relationship between the high Mn concentration / high radiogenic strontium in the Cretaceous limestones and the salt domes.

Acknowledgements

Special thanks to G. Venturelli for the comments and suggestions on a preliminary version of the manuscript. The authors very much appreciate the Associate Editor, B.J. Katz, and the two anonymous reviewers for their careful reading of the manuscript and all valuable constructive comments and suggestions.

Captions

Table 1 – Physicochemical parameters, major ion composition, trace elements concentration, and isotopic results from Awadh et al. (2018) and this study.

Table 2 – Geothermometric results in Celsius degree (°C); mineral saturation indices (SI), and carbon dioxide partial pressure as $logP(CO_2)g$ obtained by PHREECI code, version 3, along with Pitzer thermodynamic dataset at the measured temperature and water pressure conditions (Table 1). EQ 3/6 code was also used to calculate the saturation indexes of carbonates solid solution.

Figure 1 **–** A) Location map showing the studied oilfields at the Zubair zone, within the southern part of the Mesopotamia plain and to the southwest of the Zagros Foredeep Fault (ZFF); Stratigraphic correlation of the five oilfield wells penetrating four formations

(Rumaila, Mishrif, Khasib, and Tanuma) in which there is a well from each oilfield (RU287 from Rumaila South, R590 from Rumaila North, WQ87 from West Qurna, MJ20 from Majnoon, and ZB140 from Zubair oilfield); B) Typical section represents the stratigraphic setting in the study area.

Figure 2 **–** Langelier–Ludwig (A) and Brine Differentiation Plot (B) of the oilfield brines of southern Iraq (Al-Mallah, 2014; Al-Marsoumi and Abdul-Wahab, 2005; Awadh et al., 2019b; Awadh et al., 2018; Jamil, 1978) compared with shallow groundwater (Hamdan, 2017), Shatt Al-Arab River (ROPME, 2011), Shatt Al-Basrah Canal, or 'Main Drain' (Al-Mallah, 2014) and seawater. In both diagrams, concentration of the dissolved species are in equivalent/liter; dashed ellipses depict the trend of the Tigris–Euphrates River system at Qurna and Shatt Al-Arab River during the 60s (Rzóska, 1980). In (B), Mishrif Formation's brine waters from Awadh et al. (2018) are distinguished by black triangles; the five samples reprised in this study are highlighted by white crosses. The brine data from other references (Al-Mallah, 2014; Al-Marsoumi and Abdul-Wahab, 2005; Awadh et al., 2019b; Jamil, 1978) are represented by white triangles. Produced waters from hydrocarbon dehydrators are also shown for comparison (dashed field) (Al-Furaiji, 2016; Al-Shamkhani, 2013). Arrows depict possible mixing trends. In the inset, the original fields of the diagram along with evaporation paths of present-day (Boschetti, 2011; Hounslow, 1995) and Cretaceous seawater (this study) are shown. G and H depict the gypsum and halite saturation points, respectively.

Figure 3 **–** Ca-excess = 2 x $[Ca_{meas} - (Ca/Cl)_{SW} \times Cl_{meas}]/40.08$ vs. Na-defict = $[(Na/Cl)_{SW} \times Cl_{meas} - Na_{meas}] / 22.99$ diagram for oilfield waters from southern Iraq, where meas = measured, SW = seawater and Ca, Na and Cl are elemental concentrations in mg/l (Davisson and Criss, 1996). The 1Ca-2Na or 1Ca-1Na exchange arrows depict the possible paths of formation fluids in sedimentary basins during plagiocalse albitisation (Davisson and Criss, 1996). In (A) and (B) diagrams, present-day and Cretaceous seawater were used as SW-composition, respectively. In both: light gray ellipse at the origin of the plot represents the initial seawater composition (i.e. before evaporation), local groundwater and surface waters composition; dashed and dot-dashed lines depict the evaporation paths of Cretaceous and present-day seawaters, respectively. Other symbols and fields as in Figure 2.

Figure 4 **–** Base-10 logarithm of silicium versus calcium/magnesium ratio diagram of the Mishrif Formation's brines from southern Iraq (molar concentration). Dashed curves depict the simultaneous equilibria of calcite-dolomites plus quarz (light gray) or chacedony (black) calculated by PHREEQCI code and pitzer thermodynamic dataset (Parkhurst and Appelo, 2013) at the mean pressure of the five samples (27.8 MPa; Table 1).

Figure 5 **–** Activity plots for the system Na_2O-CaO-MgO-Al_2O_3-SiO_2-H_2O-CO_2 at P = 200 bar and 50 < T < 75 °C. In (A), the activity of dissolved silica has been fixed at the mean value detected in the waters, i.e.: $\log[SiO_2(aq)] = -3.32$, whereas in (B) it was buffered by chalcedony. In both diagrams: water activity at $\log[H_2O] = -0.0855$ (mean value of the local brines); aluminium buffered by kaolinite; magnesium and HCO_3^- buffered by dolomite and calcite, respectively.

Figure 6 **–** $\delta^2H(H_2O)$ vs. $\delta^{18}O(H_2O)$ diagram. Samples from this study are diffentiated for isotope composition (white-crossed gray triangles) and isotope activity (white-crossed black triangles): the former represent analytical results of water samples after vacuum distillation and IRMS; the latter represent isotope composition plus the theoretical salt effect (Horita et al., 1993) (Table 1). Water isotope composition of brines from the Mishrif Formation in Qatar are also shown for comparison (open triangles) (Danquigny et al., 2005). Dotted lines depict the linear best fits of the two ways of representation of isotope ratios in brines.

Evaporated seawaters from a closed (Gonfiantini et al., 2018) and open (McKenzie et al., 1980; Nadler and Magaritz, 1980; Robinson and Gunatilaka, 1991) system are shown for comparison. The previous published data on isotope composition of the Arabian Gulf seawater and its evaporated composition are depicted by the field with waves and forward-back curved arrows, respectively (Bagheri et al., 2014; McKenzie et al., 1980; Robinson and Gunatilaka, 1991; Yurtsever, 1994). Rainwater samples (drops) from southern Iraq (Al-Kinani et al., 2018; Ali et al., 2015; Jassem et al., 2018) and nothern Kuwait (Hadi et al., 2016) are also shown for comparison. Tigris and Euphrates samples are represented by open squares; samples out of the IMWL's (Iraq meteoric water line) prediction interval are evaporated surface water samples (arrow with slope ~ 4.3) (Ali et al., 2015; Jassem et al., 2018).

Supplementary File 1 - Calculation of the thermodynamic equilibria by Rxn tool of The Geochemist's Workbench® code (Bethke and Yeakel, 2008) and P = 20 MPa thermodynamic dataset (Boschetti et al., 2016). To reduce the variables, the activity of calcium and hydrogen was rewritten as log-ratio in the reaction and automatically rebalanced by the tool.

References

Abbas, L.K., Mahdi, T.A., 2019. Reservoir units of Mishrif Formation in Majnoon Oil field, Southern Iraq. Iraqi Journal of Science 60, 2656-2663.

Abeed, Q., Leythaeuser, D., Littke, R., 2012. Geochemistry, origin and correlation of crude oils in Lower Cretaceous sedimentary sequences of the southern Mesopotamian Basin, southern Iraq. Organic Gechemistry 46, 113-126.

Abeed, Q., Littke, R., Strozyk, F., Uffmann, A.K., 2013. The Upper Jurassic–Cretaceous petroleum system of southern Iraq: A 3-D basin modelling study. GeoArabia 18, 179-200.

Al-Ameri, T.K., Jafar, M.S., Pitman, J., 2011. Hydrocarbon generation modeling of the Basrah oil fields, Southern Iraq. University of Baghdad, Jadiriyah, AAPG Annual Convention and Exhibition. AAPG Search and Discovery, Houston, Texas.

Al-Furaiji, M., 2016. Hyper-saline produced water treatment for beneficial use. University of Twente, Gildeprint - The Netherlands.

Al-Kinani, S.A.A., Falih, A.H., Al-abidin, H.A.Z., Al-Naseri, S.K.A.A.H., 2018. Determination of the Meteoric Water Line Using Stable Isotopes in Precipitations at Several Locations In Baghdad. Iraqi Journal of Science and Technology 4, 36-42.

Al-Mallah, I.A., 2014. Assessment of the Environmental, Hydrological and Hydrogeological changes of the Main Drain, Iraq, College of Science - Department of Geology. University of Basrah, Basrah, Iraq.

Al-Marsoumi, A.M.H., Abdul-Wahab, D.S., 2005. Hydrogeochemistry of Yamama Reservoir formation water - west Qurna oil field - Southern Iraq. Basrah Journal of Science 23, 10-20.

Al-Mimar, H.S., Awadh, S.M., 2019. The Role of Chemistry of the Oil-Field Water in the Distribution of Reservoir Pressures: A Case Study of Mishrif Reservoir in the Southern Oil-Fields, Iraq. Journal of Petroleum Research & Studies 22, E52-E64.

Al-Mimar, H.S., Awadh, S.M., Al-Yaseri, A.A., Yaseen, Z.M., 2018. Sedimentary units-layering system and depositional model of the carbonate Mishrif reservoir in Rumaila oilfield, Southern Iraq. Modeling Earth Systems and Environment 4, 1449-1465.

Al-Shamkhani, M.T., 2013. Managing, Controlling and Improving the Treatment of Produced Water Using the Six Sigma Methodology for the Iraqi Oil Fields, College of Engineering and Computer Science - Department of Industrial Engineering and Management Systems. University of Central Florida, Orlando, Florida.

Al-Ziayyir, H.G.F., 2018. Mineralisation-Related Flow Heterogeneity within the Zubair Formation in the Rumaila Oilfield, Southern Iraq, Faculty of Science and Engineering. University of Manchester, Manchester.

Ali, K.K., Al-Kubaisi, Q.Y., Al-Paruany, K.B., 2015. Isotopic study of water resources in a semi-arid region, western Iraq. Environmental Earth Sciences 74, 1671-1686.

Alsharhan, A.S., Nairn, A.E.M., 1988. A review of the Cretaceous Formations in the Arabian Peninsula and Gulf: Part II. Mid-Cretacous (Wasia Group) Stratigraphy and Paleogeography. Journal of Petroleum Geology 11, 89-112.

Alyasi, A.I., Al-Jawad, S.N., Alshabender, L.Y., 2014. Geophysical Study to the Role of Salt in Creating Buzurgan Oilfield Structure, Southeast of Iraq. Iraqi Journal of Science 55, 1579-1587.

Aqrawi, A.A.M., Horbury , A.D., Sadooni, F.N., Goff, J.C., 2010. The Petroleum Geology of Iraq. Scientific Press, Beaconsfield, Bucks, UK.

Aqrawi, A.A.M., Thehni, G.A., Sherwani, G.H., Kareem, B.M.A., 1998. Mid-Cretaceous rudist-bearing carbonates of the Mishrif Formation: an important reservoir sequence in the Mesopotamian Basin, Iraq. Journal of Petroleum Geology 21, 57-82.

Awadeesian, A.M., Awadh, S.M., Al-Dabbas, M.A., Al-Maliki, M.M., Al-Jawad, S.N., Hussein, A.K.S., 2019. A modified water injection technique to improve oil recovery: Mishrif carbonate resevoirs in Southern Iraq oil fileds, case study. Iraqi Geological Journal 52, 125-146.

Awadh, S., Al-Mimar, H., Al-yaseri, A., 2019a. Potentiometric Salinity Mapping of Mishrif Oilfield Waters in (Iraq's) Southern Oil Fields, in: Chaminé, H.I., Barbieri, M., Kisi, O., Chen, M., Merkel, B.D. (Eds.), Advances in Sustainable and Environmental Hydrology, Hydrogeology, Hydrochemistry and Water Resources - Proceedings of the 1st Springer

Conference of the Arabian Journal of Geosciences (CAJG-1), Tunisia 2018. Springer Nature, Switzerland, pp. 49-52.

Awadh, S.M., Al-Auweidy, M.R., Al-Yaseri, A.A., 2019b. Hydrochemistry as a tool for interpreting brine origin and chemical equilibrium in oilfields: Zubair reservoir southern Iraq case study. Applied Water Science, 93.

Awadh, S.M., Al-Mimar, H.S., Al-Yaseri, A.A., 2018. Salinity mapping model and brine chemistry of Mishrif reservoir in Basrah oilfields, Southern Iraq. Arabian Journal of Geosciences 11.

Bąbel, M., Schreiber, B.C., 2014. Geochemistry of Evaporites and Evolution of Seawater in: Holland, H.D., Turekian, K.K. (Eds.), Treatise on Geochemistry, 2nd ed. Elsevier, Printed and bound in Italy, pp. 483-560.

Bagheri, R., Nadri, A., Raeisi, E., Eggenkamp, H.G.M., Kazemi, G.A., Montaseri, A., 2014. Hydrochemical and isotopic ($\delta^{18}O$, $\delta^{2}H$, $^{87}Sr/^{86}Sr$, $\delta^{37}Cl$ and $\delta^{81}Br$) evidence for the origin of saline formation water in a gas reservoir. Chemical Geology 384, 62-75.

Basilici, M., Mazzoli, S., Megna, A., Santini, S., Tavani, S., 2020. 3-D Geothermal Model of the Lurestan Sector of the Zagros Thrust Belt, Iran. Energies 13.

Bethke, C.M., Yeakel, S., 2008. The Geochemist's Workbench® - Release 7. GWB Essentials Guide, Hydrogeology Program. University of Illinois.

Bordenave, M.L., 2008. The origin of the Permo-Triassic gas accumulations in the Iranian Zagros foldbelt and contiguous offshore areas: a review of the Palaeozoic petroleum system. Journal of Petroleum Geology 31, 3-42.

Bordenave, M.L., Hegre, J.A., 2010. Current distribution of oil and gas fields in the Zagros Fold Belt of Iran and contiguous offshore as the result of the petroleum systems, in: Leturmy, P., Robin, C. (Eds.), Tectonic and Stratigraphic Evolution of Zagros and Makran during the Mesozoic–Cenozoic. The Geological Society of London, London, pp. 291-353.

Boschetti, T., 2011. Application of brine differentiation and Langelier–Ludwig plots to fresh-to-brine waters from sedimentary basins: Diagnostic potentials and limits. Journal of Geochemical Exploration, 108, 126-130.

Boschetti, T., Angulo, B., Cabrera, F., Vásquez, J., Montero, R.L., 2016. Hydrogeochemical characterization of oilfield waters from southeast Maracaibo Basin (Venezuela): Diagenetic effects on chemical and isotopic composition. Marine and Petroleum Geology 73, 228-248.

Boschetti, T., Cifuentes, J., Iacumin, P., Selmo, E., 2019. Local Meteoric Water Line of Northern Chile (18°S - 30°S): An application of error-in-variables regression to the oxygen and hydrogen stable isotope ratio of precipitation. Water 11

Boschetti, T., Toscani, L., Salvioli Mariani, E., 2015. Boron isotope geochemistry of Na- bicarbonate, Na- chloride, and Ca- chloride waters from the Northern Apennine Foredeep basin: other pieces of the sedimentary basin puzzle. Geofluids 15, 546-562.

Boschetti, T., Toscani, L., Shouakar-Stash, O., Iacumin, P., Venturelli, G., Mucchino, C., Frape, S.K., 2011. Salt waters of the Northern Apennine Foredeep Basin (Italy): origin and evolution. Aquatic Geochemistry 17, 71-108.

Clesceri, L.S., Greenberg, A.E., Eaton, A.D., 1999. Method 4500-SiO_2 D, Heteropoly Blue Method, Standard methods for the examination of water and wastewater, 20th. American Public Health Association, American Water Works Association, Water Environment Federation, Washington.

Danquigny, J.A., Matthews, J., Noman, R., Mohsen, A., 2005. Assessment of interwell communication in the carbonate Al Khalij oil field using isotope ratio water sample analysis, International Petroleum Technology Conference. IPTC, Doha, Qatar

Davisson, M.L., Criss, R.E., 1996. Na-Ca-Cl relations in basinal fluids. Geochimica et Cosmochimica Acta 60, 2743-2752.

Deville de Periere, M., 2011. Origine sédimento-diagénétique de réservoirs carbonatés microporeux: exemple de la formation Mishrif (Cénomanien) du Moyen-Orient. Université de Bourgogne.

Ghalib, H.B., Almallah, I.A.R., 2017. Scaling simulation resulting from mixing predicted model between Mishrif formation water and different waters injection in Basrah oil field, southern Iraq. Modeling Earth Systems and Environment 3, 1557-1569.

Giggenbach, W.F., 1991. Chemical Techniques in geothermal exploration, in: D'Amore, F. (Ed.), Application of Geochemistry in Geothermal Reservoir Development. UNITAR, Rome, Italy, pp. 119–144.

Gonfiantini, R., 1965. Effetti isotopi nell'evaporazione di acque salate. Atti della Società Toscana di Scienze Naturali - Memorie, Serie A 72, 1-22.

Gonfiantini, R., Wassenaar, L.I., Araguas-Araguas, L., Aggarwal, P.K., 2018. A unified Craig-Gordon isotope model of stable hydrogen and oxygen isotope fractionation during fresh or saltwater evaporation. Geochimica et Cosmochimica Acta 235, 224-236.

Grabowski Jr., G.J., 2014. Iraq, in: Marlow, L., Kendall, M.C., Yose, L.A. (Eds.), Petroleum systems of the Tethyan region. The American Association of Petroleum Geologists, Tulsa, OK U.S.A., pp. 379–467.

Gregory, R.T., Taylor Jr, H.P., 1981. An oxygen isotope profile in a section of Cretaceous oceanic crust, Samail Ophiolite, Oman: Evidence for $\delta^{18}O$ buffering of the oceans by deep (>

5 km) seawater- hydrothermal circulation at mid- ocean ridges. Journal of Geophysical Research: Solid Earth 86, 2737-2755.

Hadi, K., Kumar, U.S., Al-Senafy, M., Bhandary, H., 2016. Environmental isotope systematics of the groundwater system of southern Kuwait. Environmental Earth Sciences 75.

Hajikazemi, E., Al-Aasm, I.S., Coniglio, M., 2017. Diagenetic history and reservoir properties of the Cenomanian-Turonian carbonates in southwestern Iran and the Persian Gulf. Marine and Petroleum Geology 88, 845-857.

Hajikazemi, E., Al- Aasm, I.S., Coniglio, M., 2012. Chemostratigraphy of Cenomanian–Turonian carbonates of the Sarvak Formation, southern Iran. Journal of Petroleum Geology 35, 187-205.

Hamdan, A.N.A., 2017. The use of water quality index to evaluate groundwater quality in west of Basrah wells. Kufa Journal of Engineering 8, 51-64.

Holser, W., 1979. Trace elements and isotopes in evaporites, in: Burns, R.G. (Ed.), Marine Minerals. De Gruyter - Mineralogical Society of America, Berlin, Boston, pp. 295–346.

Hönisch, B., Ridgwell, A., Schmidt, D.N., Thomas, E., Gibbs, S.J., Sluijs, A., Zeebe, R., Kump, L., Martindale, R.C., Greene, S.E., Kiessling, W., Ries, J., Zachos, J.C., Royer, D.L., Barker, S., Marchitto Jr., T.M., Moyer, R., Pelejero, C., Ziveri, P., Foster, G.L., Williams, B., 2012. The geological record of ocean acidification. Science 335, 1058-1063.

Horita, J., 2009. Isotopic evolution of saline lakes in the low-latitude and polar regions. Aquatic Geochemistry 15, 43-69.

Horita, J., Cole, D.R., Wesolowski, D.J., 1993. The activity-composition relationship of oxygen and hydrogen isotopes in aqueous salt solutions: II. Vapor-liquid water equilibration of mixed salt solutions from 50 to 100 C and geochemical implications. Geochimica et Cosmochimica Acta 57, 4703-4711.

Hounslow, A.W., 1995. Water Quality Data Analysis and Interpretation. Lewis Publishers, Boca Raton, New York.

Jamil, A.K., 1978. Hydrochemical and Hydrodynamic Zones and the Probable Direction of Water Flow within Zubair Reservoir of Zubair and Rumaila Oil Fields (Southern Iraq). Geologisches Jahrbuch, Reihe D, D25, 199-211.

Jassem, A.A., Nada, K.B., Abdualamer, Z.S., 2018. Using ^{18}O, ^{2}H isotopes to study the effect of fish lake on sueface water in Al-Azezeya, Kut Governatorate, Iraq. The Iraqi Geological Journal 51, 149-156.

Jassim, S.Z., Buday, T., 2006. Units of the Stable Shelf, in: Jassim, S.Z., Goff, J.C. (Eds.), Geology of Iraq. Dolin, Prague and Moravian Museum, Brno. Czech Republic, pp. 53-72.

Kharaka, Y.K., Mariner, R.H., 1989. Chemical geothermometers and their application to formation waters from sedimentary basins, in: Naeser, N.D., McCollin, T.H. (Eds.), Thermal history of sedimentary basins. Springer-Verlag, New York, pp. 99–117.

Kim, S.T., O'Neil, J.R., 1997. Equilibrium and nonequilibrium oxygen isotope effects in synthetic carbonates. 61 Geochimica et cosmochimica acta, 3461-3475.

Knauth, L.P., Beeunas, M.A., 1986. Isotope geochemistry of fluid inclusions in Permian halite with implications for the isotopic history of ocean water and the origin of saline formation waters. Geochimica et Cosmochimica Acta 50, 419-433.

Konyuhov, A.I., Maleki, B., 2006. The Persian Gulf Basin: Geological history, sedimentary formations, and petroleum potential. Lithology and Mineral Resources 41, 344–361

Lemarchand, D., Gaillardet, J., Lewin, E., Allegre, C.J., 2002. Boron isotope systematics in large rivers: implications for the marine boron budget and paleo-pH reconstruction over the Cenozoic. Chemical Geology 190, 123-140.

Lowenstein, T.K., Hardie, L.A., Timofeeff, M.N., Demicco, R.V., 2003. Secular variation in seawater chemistry and the origin of calcium chloride basinal brines. Geology 31, 857-860.

Mahdi, T.A., Aqrawi, A.A., Horbury, A.D., Sherwani, G.H., 2013. Sedimentological characterization of the mid-Cretaceous Mishrif reservoir in southern Mesopotamian Basin, Iraq. GeoArabia 18, 139-174.

McArthur, J.M., 2010. Strontium isotope stratigraphy, in: Ratcliffe, K.T., Zaitlin, B.A. (Eds.), Application of modern stratigraphic techniques: theory and case histories. SEPM Society for Sedimentary Geology, Tulsa, Oklahoma, pp. 129–142.

McArthur, J.M., Howarth, R.J., Shields, G.A., 2012. Strontium isotope stratigraphy, in: Gradstein, F.M., Ogg, J.G., Schmitz, M.D., Ogg, G.M. (Eds.), The geologic time scale 2012. Elsevier, Oxford, pp. 127–144.

McKenzie, J.A., Hsü, K.J., Schneider, J.F., 1980. Movement of subsurface waters under the sabkha Abu Dhabi, UAE, and its relation to evaporative dolomite genesis, in: Zenger, D.H., Dunham, J.B., Ethington, R.L. (Eds.), Concepts and Models of Dolomitization. SEPM Society for Sedimentary Geology, Tulsa, Oklahoma, USA, pp. 11-30.

Mortazavi, M., Heuss-Assbichler, S., Shahri, M., 2017. Hydrothermal systems in the salt domes of south Iran. Procedia Earth and Planetary Science 17, 913-916.

Murris, R.J., 1980. Middle East: stratigraphic evolution and oil habitat. AAPG Bulletin 64, 597-618.

Nadler, A., Magaritz, M., 1980. Studies of marine solution basins isotopic and compositional changes during evaporation, in: Nissembaum, A. (Ed.), Hypersaline Brines and Evaporitic Environments. Elsevier, Amsterdam, The Netherlands, pp. 115-129.

Navidtalab, A., Rahimpour-Bonab, H., Huck, S., Heimhofer, U., 2016. Elemental geochemistry and strontium-isotope stratigraphy of Cenomanian to Santonian neritic carbonates in the Zagros Basin, Iran. Sedimentary Geology 346, 35-48.

Parkhurst, D.L., Appelo, C.A.J., 2013. Description of input and examples for PHREEQC version 3: a computer program for speciation, batch-reaction, one-dimensional transport, and inverse geochemical calculations Techniques and Methods. US Geological Survey, Reston, VA, p. This report is Chapter 43 of Section A: Groundwater in Book 46 Modeling Techniques.

Rahimpour- Bonab, H., Mehrabi, H., Navidtalab, A., Omidvar, M., Enayati- Bidgoli, A.H., Sonei, R., Sajjadi, F., Amiri-Bakhtyar, H., Arzani, N., Izadi- Mazidi, E., 2013. Palaeo- exposure surfaces in Cenomanian–santonian carbonate reservoirs in the Dezful embayment, SW Iran. Journal of Petroleum Geology 36, 335-362.

Robinson, B.W., Gunatilaka, A., 1991. Stable isotope studies and the hydrological regime of sabkhas in southern Kuwait, Arabian Gulf. Sedimentary Geology 73, 141-159.

ROPME, 2011. The Marshes-Shatt al-Arab- Gulf System, in: Environment, R.O.f.t.P.o.t.M. (Ed.). Marine Science Centre – University of Basra in Cooperation with Ministry of Environment Iraq, p. 102.

Rosenthal, E., 1997. Thermomineral waters of Ca-chloride composition: review of diagnostics and of brine evolution. Environmental Geology 32, 245-250.

Ryb, U., Eiler, J.M., 2018. Oxygen isotope composition of the Phanerozoic ocean and a possible solution to the dolomite problem. Proceedings of the National Academy of Sciences 115, 6602-6607.

Rzóska, J., 1980. Euphrates and Tigris, Mesopotamian ecology and destiny. Dr. W. Junk bv Publishers, The Hague The Netherlands.

Sadooni, F.N., 2005. The nature and origin of Upper Cretaceous basin-margin rudist buildups of the Mesopotamian Basin, southern Iraq, with consideration of possible hydrocarbon stratigraphic entrapment. Cretaceous Research 26, 213-224.

Sadooni, F.N., Aqrawi, A.A.M., 2000. Cretaceous sequence stratigraphic and petroleum potential of the Mesopotamian basin, Iraq, in: Alsharhan, A.S., Scott, R.W. (Eds.), Middle East Models of Jurassic/Cretaceous Carbonate Systems. SEPM Society for Sedimentary Geology, Tulsa, Oklahoma, USA, pp. 315-334.

Sanjuan, B., Millot, R., Asmundsson, R., Brach, M., Giroud, N., 2014. Use of two new Na/Li geothermometric relationships for geothermal fluids in volcanic environments. Chemical Geology 389, 60-81.

Sessions, A.L., 2016. Factors controlling the deuterium contents of sedimentary hydrocarbons. Organic Geochemistry 96, 43–64.

Singh, P., 2012. New Insights to the Implications of Salt Tectonics in the Northern Part of Kuwait Arch: An Integrated Modeling Study, First EAGE Workshop on Iraq-Hydrocarbon Exploration and Field Development. European Association of Geoscientists & Engineers (EAGE), Istanbul, Turkey

Sissakian, V., Abdul Ahad, A., Al-Ansari, N., Knutsson, S., 2017. Geomorphology, Geology and Tectonics of Jabal Sanam, Southern Iraq. Journal of Earth Sciences and Geotechnical Engineering 7, 97-113.

Sorbie, K.S., Mackay, E.J., 2000. Mixing of injected, connate and aquifer brines in waterflooding and its relevance to oilfield scaling. Journal of Petroleum Science and Engineering. 27, 85-106.

Taha, T.M., Abdullah, E.J., 2019. Reconstruction of Paleo depth and Paleo temperature from C-O stable isotope records of Mishrif Formation, southern Iraq. Iraqi Journal of Science 60, 1730-1742.

Vengosh, A., Starinsky, A., Kolodny, Y., Chivas, A.R., Raab, M., 1992. Boron isotope variations during fractional evaporation of sea water: new constraints on the marine vs. nonmarine debate. Geology 20, 799–802.

Wang, Y., Huang, C., Sun, B., Quan, C., Wu, J., Lin, Z., 2014. Paleo-CO_2 variation trends and the Cretaceous greenhouse climate. Earth-Science Reviews 129, 136-147.

Wolery, T.W., Jarek, R.L., 2003. EQ3/6, version 8.0—software user's manual. Civilian radioactive waste management system, Management & Operating Contractor, Sandia National Laboratories, Albuquerque, New Mexico.

Yurtsever, Y., 1994. Role of environmental isotopes in studies related to salinization processes and salt water intrusion dynamics, 13th Salt Water Intrusion Meeting - Session 3: Hydrogeochemical and environmental isotope studies. Mixing zone. Characterization of the origin and dynamics of salt and brackish waters, Cagliari, Italy, pp. 5-10.

Zheng, Y.-F., 1999. Oxygen isotope fractionation in carbonate and sulfate minerals. Geochemical Journal 33, 109-126.

Chemical and isotope composition of the oilfield brines from Mishrif Formation (southern Iraq): Diagenesis and geothermometry

Tiziano Boschetti[1], Salih Muhammad Awadh[2], Heba Sadoon Al-Mimar[2], Paola Iacumin[1], Lorenzo Toscani[1], Enricomaria Selmo[1], Zaher Mundher Yaseen[3,*]

[1] Department of Chemistry, Life Sciences and Environmental Sustainability, University of Parma, Parco Area delle Scienze 157/A, 43124 Parma, Italy

[2] Department of Geology, College of Science, University of Baghdad, Baghdad, Iraq

[3] Sustainable Developments in Civil Engineering Research Group, Faculty of Civil Engineering, Ton Duc Thang University, Ho Chi Minh City, Vietnam

*Corresponding authors: Zaher Mundher Yaseen

Email: yaseen@tdtu.edu.vn

Abstract

This paper focuses on the geochemical composition and isotope geochemistry of brines in the Cenomanian–Turonian carbonate Mishrif reservoir of southern Iraq. Main dissolved constituents, trace elements, $\delta^{2}H$ and $\delta^{18}O$, $^{87}Sr/^{86}Sr$, mineral saturation indices and thermodynamic calculations were investigated in formation waters from the Mishrif Formation to obtain a better understanding of brine evolution and diagenetic effects over geological time. Previous published $\delta^{11}B$ data were also reinterpreted as a geothermometer tool. The results are compared with previous published data for local oilfields and coeval formations in the Arabian Gulf. The Mishrif brine has a marine origin and is diagenetically modified to Ca-excess and Na-deficit. Formation waters are quartz supersaturated and are in equilibrium with chalcedony and calcite-dolomite in the temperatures range of 50–75°C, which is also confirmed by calcite-water oxygen isotope fractionation and $\delta^{11}B$ geothermometer. The potential role of clays in conditioning brine chemistry during diagenetic processes was highlighted by activity diagrams; in particular, their adsorption/exchange effect on sodium could explain the lower temperature obtained by the Na/Li geothermometer (42 ± 6 °C). The $\delta^{2}H$ and $\delta^{18}O$ values show that oxygen isotope composition of the brines was isotopically more affected by interaction with limestone during diagenesis than seawater evaporation. The main effect is an ^{18}O-enrichment on the brine starting from the SMOW value. Locally, dilution by present-day meteoric water was also detected (Rumaila South), which is shifted towards the local meteoric water line. The strontium isotope ratios range from 0.707713 to 0.707749 and correspond to a marine strontium of late Cenomanian–early Maastrichtian age, except for the Majnoon sample, which shows a more radiogenic value (0.708043). Radiogenic strontium and gypsum and anhydrite saturation indices of the Majnoon sample could indicate the contribution of calcium and sulphate from the strontium-rich sulphate minerals of the Cambrian salt domes occurring in the oilfields of southern Iraq.

The higher manganese concentration (4 mg/l) and the slightly higher temperature inferred by geothermometers (up to 74 °C) in comparison with present-day could indicate that the Majnoon brine is a hot fluid, probably related to a deeper structure such as the Zagros Foredeep Fault.

Keywords: Oilfield waters; chemical composition; geothermometry; oxygen and hydrogen stable isotope ratios; strontium isotopes.

1. Introduction

In the Jurassic–Cretaceous petroleum system of southern Iraq, hydrocarbons are mainly trapped in Lower Cretaceous sandstone and carbonate reservoirs. Crude oil is generated from the organic-rich Upper Jurassic (Sargelu and Sulaiy formations) changing the Lower Cretaceous carbonates of the Yamama Formation and the Zubair Formation, a clastics reservoir (Abeed et al., 2012; Abeed et al., 2013). The chemical composition of formation waters from the Yamama reservoir in the Zubair and North/South Rumaila oilfields is mainly composed of chloride (up to 143,589 ppm) with a salinity 6.2 times higher than seawater (Jamil, 1978), as for West Qurna oilfield, salinity 7.3 times higher than seawater and dominated by 191,700 ppm of chloride (Al-Marsoumi and Abdul-Wahab, 2005). These prior works utilized brine chemistry but did not address the evolution of the reservoir brine, as they relied mainly on cations and anions without considering isotopes. More recently, the boron stable isotope ratio of the brine from the Mishrif reservoir has given a seawater signature (Awadh et al., 2019a; Awadh et al., 2018) and highlighted the role of salinity in generating the formation pressure and controlling the fluid flow (Al-Mimar and Awadh, 2019). The developing of the oilfield brines over the geological time and its response to the flooding and diagenesis have a significant impact on petroleum reservoir quality, but this subject has not yet been investigated.

The diagenetic effects on brine waters can be evaluated by comparing the Na, Ca and Cl concentrations of the brine with those of seawater and with the so-called basinal fluid line in the Ca-excess versus Na-deficit binary diagram (Davisson and Criss, 1996). However, in this plot the interpretation could be misguided because: (i) the reference basinal fluid line takes into account only plagioclase albitisation, often without checking the real thermodynamic equilibria state of the involved waters; and ii) modelling involves the current seawater composition disregarding that of past periods (Bąbel and Schreiber, 2014; Lowenstein et al., 2003). A combination of isotope parameters as O-H stable isotope ratios and $^{87}Sr/^{86}Sr$ was proposed by Danquigny et al. (2005) to evaluate the effect of water flooding in the Mishrif Formation water of Qatar. However, in that work, seawater evaporation, the isotope salt effect (Horita et al., 1993), and the contribution of radiogenic strontium to the limestones of the Mishrif Formation were not considered.

The objectives of this research are: i) to investigate the origin of the oilfield waters; ii) to evaluate the composition of oilfield waters over time; and iii) to trace the influence of diagenesis and any geothermal effects on the brine. This investigation considers the above described effects and processes in the Mishrif Formation brines by reinterpreting the previously published main chemical constituents, along with new and original data on trace elements, oxygen and hydrogen water isotope ratio, the $^{87}Sr/^{86}Sr$ ratio, and thermodynamic calculations. Moreover, the previously published data of boron isotope ratio $\delta^{11}B$ (Awadh et al., 2019a; Awadh et al., 2018) are here reinterpreted as a geothermometer tool, and are results compared with those obtained from chemical geothermometers. The main research contribution is to obtain better understanding of the oilfield brines evolution.

2. Geological setting

2.1. Oilfield locations, main geological features and tectonics

The studied oilfields, Rumaila South (RU), Rumaila North (R), West Qurna (WQ), Zubair (ZB) and Majnoon (MJ) are located in southern part of Iraq (Jassim and Buday, 2006) (Fig. 1A). The Mesopotamian zone extends from middle to southern Iraq as a relatively flat terrain with a gradient of less than 10 cm/km in the north-west to the Arabian Gulf. The zone was probably uplifted during Hercynian deformation but was subject to subsidence from the Late Permian onwards (Jassim and Buday, 2006). The oilfields are located in the Zubair zone (Grabowski Jr., 2014; Sadooni and Aqrawi, 2000), southern part of the Mesopotamia plain (Fig. 1A), an area characterized by the presence of a gentle subsurface succession of anticlinal and synclinal structures. These structures form giant hydrocarbon traps: Rumaila South (37 km length, 16 km width), Rumaila North (40 km, 13.5 km), West Qurna (35 km, 8 km) and Majnoon (48 km, 10 km).

From the interpretation of gravity and magnetic data, Alyasi et al. (2014) mentioned that the presence of anticlinal structures is due to the effect of the evaporites of the Late Jurassic Gotnia Formation and Late Ediacaran – Early Cambrian Hormuz Formation in addition to other tectonic forces, where salts moves upward by buoyant forces and the denser rocks remain below them. To the north of the Arabian Gulf, huge salt-gypsum domes are exposed at a surface coexisting with a mixture of igneous and metamorphic rocks peeled off from the Precambrian crystalline basement (Mortazavi et al., 2017). Jabal Sanam is one of the salt diapirs in southern Iraq / northern Kuwait border (Fig. 1); it is an extension of the Hormuz Formation, located in Iran at the northern part of the Arabian Gulf, which contains more than 200 salt domes composed of sequences of evaporates, shales, siltstones and carbonates (Mortazavi et al., 2017). The role of tectonic events (extensional faulting) and differential loading of sedimentary cover above the mobile salt layer are the main triggering factors of the salt diapirism (Singh, 2012). In particular, the Permo-Triassic Tethyan rifting, the Cretaceous-Paleogene obduction and the compressive events associated with basement

reactivation of north-south Arabian trends could have started the episodic salt diapir activity in the area of this study (Singh, 2012). However, traces of a neotectonic reactivation were also documented (Sissakian et al., 2017).

The Zubair zone is a southern part of the Mesopotamian Basin that is located close to the junction of the Arabian Shelf and Iranian continental block. Collision of these plates at the Mesozoic-Cenozoic boundary produced the Zagros Foredeep fault and the Mesopotamian Basin, which is a member of the Arabian Gulf Basin (Konyuhov and Maleki, 2006). During the Mesozoic and Cenozoic, the study area was a tropical region, with organic-rich carbonates or organic-rich argillaceous sediments being deposited. Good-quality source rocks were preserved in different intervals of geological time, particularly during the Mesozoic. For example (Fig. 1B): the Alan Formation in the Middle Jurassic; the Sargelu, Najmah and Sulaiy formations are the source rocks in the Upper Jurassic; the Yamama Formation is a reservoir and productive carbonate and the Zubair Formation is a reservoir and productive sand in the Lower Cretaceous; the Ratawi, Shuaiba and Nahr Umr formations are carbonate reservoirs in the Lower Cretaceous. The Mauddud, Ahmadi and Rumaila formations are the mainly carbonate reservoirs in the Cenomanian. The Mishrif Formation is a main carbonate reservoir of the Cenomainan-Touronian (Fig. 1B). The Khasib and Tanuma formations are poor reservoirs. Tectonic fracturing of younger higher carbonate permits vertical migration of hydrocarbons into anticlines under efficient evaporitic seals. The regional evaporite seal is Gotnia Formation in the Upper Jurassic, and Fat'ha Formation in the Tertiary (Fig. 1B).

2.2. Stratigraphy, paleogeography and mineralogy

The Mishrif Formation is the main productive reservoir in southern Iraq, the United Arab Emirates, Oman, and Qatar. It was deposited in a shallow environment on the Rumaila Formation conformity. Its upper contact is unconformable with the Khasib Formation, representing a regression in the Turonian-Campanian age (Al-Mimar et al., 2018;

Awadeesian et al., 2019). It is represented by a unique lithostratigraphic unit regionally deposited in a fluctuating environment of shallow to deep-water reflecting the tectonic activity in the area (Alsharhan and Nairn, 1988). The carbonate rocks are composed of bioclastic particles (algae, rudist and coral reef) and represent the main facies of the Mishrif Formation. In terms of mineralogy, the Mishrif Formation is mainly composed of calcite (90% av.), with heterogeneous distribution of small amounts of dolomite, kaolinite, chlorite, authigenic quartz and clays (smectites and mixed layers) that do not exceed 10% (Al-Mimar et al., 2018). Southwardly, facies change to distal mid-ramp and proximal mid-ramp deposits and grade into outer-ramp deposits (Aqrawi et al., 1998). Eastwardly, close to the Zagros Foredeep Fault (ZFF) on the border with Iran, the Mishrif Formation is thicker (up to 400 m) and deeper (up to 3000 m) (Abbas and Mahdi, 2019; Mahdi et al., 2013). In particular, thick lagoonal units were deposited in the Majnoon field, implying a paleogeographic change in the eastern part of the study area where carbonate production caught up with the rising sea level until the filling of accommodation space with lagoonal deposits (Mahdi et al., 2013). The movement of the Hormuz Formation's salts was particularly important in southern Iraq (Murris, 1980). Sadooni (2005) suggested that rudist build-ups in the Baṣrah area nucleated on the crests of growing salt structures. When the build-ups reached wave-base, they were eroded and rudist fragments were reworked, transported and dispersed to form bioclastic packstone/grainstones (Aqrawi et al., 2010).

3. Methodology

3.1. Chemical and isotope analyses

Physicochemical parameters and major ion composition of five formation water samples from Rumaila South (RU287), Rumaila North (R590), West Qurna (WQ87), Majnoon (MJ20), and Zubair (ZB140) oilfields were reprised from Awadh et al. (2018) (mean values

and standard deviations at N = 28) and reinterpreted to investigate diagenesis and the temperature of the system using geothermometry. In this study, trace elements (total sulphur, Ba, Li, Fe, Mn, Rb, Sr) were analysed at the ALS Group Laboratory in Seville (Spain) using Inductively Coupled Plasma-Atomic Emission Spectroscopy (ICP-AES; ALS analytical code ME-ICP14L) after filtration and acidification by nitric acid. The dissolved silica as $SiO_2(aq)$ was analysed using the heteropoly blue spectrophotometric method (Clesceri et al., 1999) on filtered and diluted (1:5 by 18 MOhm ASTM Type 1 water) samples. The delta isotope values of hydrogen and oxygen of water molecules in ‰ versus V-SMOW reference standard $\delta^2H(H_2O)_c$ and $\delta^{18}O(H_2O)_c$, respectively, were obtained; where subscript 'c' represents the 'composition' scale (Horita et al., 1993). These isotope measurements were conducted by the H_2-H_2O and CO_2-H_2O gas equilibration isotope ratio mass spectrometry (IRMS) method on the vacuum-distilled samples (Boschetti et al., 2011). The salt effect parameter $10^3 ln\Gamma$ of the brines was calculated taking into account the chemical composition and the temperature of the samples by PHREEQCI code, version 3, with the Pitzer thermodynamic database (Boschetti et al., 2011; Horita et al., 1993; Parkhurst and Appelo, 2013). According to Horita et al. (1993), the delta activity of hydrogen and oxygen, $\delta^2H(H_2O)_a$ and $\delta^{18}O(H_2O)_a$, respectively, was obtained summing the salt effect parameter and the delta isotope composition of hydrogen and oxygen.

The strontium isotope ratios, $^{87}Sr/^{86}Sr$, of the brines were obtained using thermal ionization mass spectrometry (TIMS). Prior to the analytical process, separation of Sr from the matrix bulk elements, and especially from Rb, was executed using heat plate evaporation with Teflon® vials at 80°C, followed by chromatographic extraction using Sr-Resin™ (TrisKem International) (crown-ether (4, 4' (5')-di-t-butylcyclohexano-18-crown-6). The final Sr fraction was recovered from the bulk using HNO_3 0.05M as eluent, then evaporated on a heat plate at 80°C and introduced into the mass spectrometer. Possible ^{87}Rb interferences

were corrected in the Sr analysis and the $^{87}Sr/^{86}Sr$ ratio was normalised in order to correct for mass fractionation, taking into account a reference value of $^{86}Sr/^{88}Sr = 0.1194$. The $^{87}Sr/^{86}Sr$ results were normalised to NBS SRM 987 (National Bureau of Standards Standard Reference Material 987 – strontium carbonate). Internal precision was 3×10^{-6}.

3.2. Thermodynamic calculations

PHREEQCI code and Pitzer thermodynamic dataset were also used to define:

i) the mineral-water saturation indices SI = log(IAP/K), where IAP and K are the ion activity product of the dissolved constituents and K is the mineral solubility product in a specific reaction, respectively, and the partial pressure of carbon dioxide by the Peng–Robinson equation of state (Parkhurst and Appelo, 2013);

ii) a geothermal model based on multimineral equilibria.

Results were compared to previously published chemical and isotopic geothermometers specific for sedimentary brines (Boschetti et al., 2015; Kharaka and Mariner, 1989; Sanjuan et al., 2014). The calculated activity of the dissolved constituents was also used to calculate the saturation index of a carbonate solid solution made of calcite, magnesite, rhodochrosite, siderite and strontianite by EQ3/6 code, version 8 (Wolery and Jarek, 2003).

The Geochemist's Workbench® code (GWB), version 7.0.6 (Bethke and Yeakel, 2008), was used to calculate the evaporation path of Cretaceous seawater using the React tool, HMW thermodynamic database, and the main chemical composition of seawater during that period (Bąbel and Schreiber, 2014). According to Bąbel and Schreiber (2014), a chloride concentration of present-day seawater (565 mmol kg^{-1} H_2O) was taken as a reference; then chloride concentration was charge-balanced, taking into account other main constituents and pH = 7.5 (Hönisch et al., 2012), and a $\log PCO_2(g) = -3$ was settled during evaporation. This

latter corresponded to a mean concentration of 1000 ppmv of CO_2 in the Cretaceous atmosphere (Hönisch et al., 2012; Wang et al., 2014).

Finally, activity diagrams using a thermodynamic database of the minerals and dissolved constituents, recalculated at a pressure of 20 MPa, were plotted using the Act tool of the GWB-code (Boschetti et al., 2016). The Rxn tool of the same code was also used to check the thermodynamic equilibria of specific reactions.

4. Results and Discussion

The physicochemical and isotope parameters are reported in Table 1. The recalculated main chemical composition in equivalents per liter of formation water from the southern region of Iraq shows a Cl-Na composition. In particular, the Na/Cl equivalent ratios range span between 0.77 and 0.91, with a mean of 0.83 ± 0.05, which is similar to that of present-day seawater (0.86). The Ca/(SO_4 + HCO_3) equivalent ratios of the brines are largely over 1, with a mean of 44 ± 19 and a range between 15 and 78. Therefore, brines can be classified also as Ca-Cl, according to Rosenthal (1997). The mean measured temperature of the water sampled in the Mishrif Formation is 65 ± 2 °C (N = 28) (Awadh et al., 2018). Between the investigated trace elements, the concentration of barium and manganese are higher in Majnoon (5.43 and 4.47 mg/l, respectively) in comparison with the range of the samples from the other oilfields (1.44-1.79 and 0.10-0.13 mg/l, respectively). All samples showed supersaturation in calcite, aragonite, and dolomite (Table 2). Barite and anhydrite are also supersaturated in all but one sample (RU287). Finally, waters are in equilibrium with chalcedony and oversaturated in quartz.

4.1 Chemical composition: diagenesis and geothermometry

According to the previous published works on southern Iraq oilfields (Awadh et al., 2019a; Awadh et al., 2018), the above described chemical ratios of Na/Cl = 0.83 ± 0.05 and Ca/(SO_4

+ HCO_3) = 44 ± 19 are typical of marine origin formation waters that have undergone chemical modification due to diagenesis (Boschetti et al., 2011; Rosenthal, 1997). The Langelier–Ludwig and brine differentiation diagrams (Boschetti, 2011; Hounslow, 1995) of Figure 2 depict the distinct composition of the oilfield brines in comparison with the local shallow groundwater (Hamdan, 2017) and surface waters (Al-Mallah, 2014; ROPME, 2011; Rzóska, 1980). Surface water (Ghalib and Almallah, 2017), water produced from crude oil dehydration (Al-Shamkhani, 2013) or a mixture of both were used in the oilfields for water-flooding purposes. In Figure 2A, the brine samples from this study and literature are grouped in a narrow field, whereas in the brine differentiation plot (Figure 2B), brines are displaced between the evaporation curve of Cretaceous seawater and the produced waters from dehydrators (Al-Furaiji, 2016; Al-Shamkhani, 2013). Similarly to the Cretaceous formation brines in Venezuela (Boschetti et al., 2016), most of the studied brines affected by diagenesis show a Ca-excess and Na-deficit and seem to follow the typical Ca-Na exchange trend of the so-called basinal fluid line (Davisson and Criss, 1996) (Figure 3). Sample RU287 was probably affected by dolomitization and then by mixing with waters produced from crude dehydrators ("produced water" field in Figure 3). The hottest (115°C) water sample from the deeper Zubair sandstone indicates that the chemical effects of Ca-Na reactions (Al-Marsoumi and Abdul-Wahab, 2005), most probably due to albitisation, are more pronounced at higher temperatures (Figure 3A). Different from the Mishrif Formation, albite was found in the Zubair Formation (Al-Ziayyir, 2018). Moreover, from a theoretical point of view, the diagenetic effects could be more or less pronounced if the variability of the seawater composition in the past was considered. If Cretaceous seawater is used as a reference instead of present-day seawater, the oilfield brines are more clustered towards the axes origin of Figure 3B (which coincides with the composition of less saline surface water) or towards the "produced water" fields. The dolomitization process seems to have had a greater role in the

Ca-excess of the waters (Figure 3B). However, the geothermal modelling indicated in Figure 4, also suggests that calcite-dolomite equilibration occurred along with chalcedony instead of quartz. In that diagram, all but one sample are clustered between 50 and 75°C isotherms, a range that includes the temperatures of 64 ± 5°C (N = 9) and 64 ± 7°C (N = 5) obtained by Mg-Li and chalcedony geothermometers, respectively — the latter corrected for dissolved silica activity and pressure (Kharaka and Mariner, 1989) (Table 2). The exception is represented by sample MJ20 (Majnoon oilfield), which is shifted towards the quartz-dolomite (ordered) model (Figure 4) and shows the lowest temperature from quartz and chalcedony from geothermometric equations (Table 2). Such an apparent convergence between quartz and chalcedony is probably attributable to the greater depth and pressure in the MJ20 borehole (Table 1), conditions that could enhance simultaneous equilibria between the fluid and the two mineral phases (Giggenbach, 1991). For the MJ20 sample, a mean value of 70.5°C between the geothermometric equations of quartz and chalcedony shows a good agreement with the 68°C obtained from the Mg-Li geothermometer (Table 2).

Globally, the mean inferred temperature of the brines are quite similar to the mean temperature measured at depth, confirming that the present-day borehole temperatures are not so different from those reached during Neogene burial (Abeed et al., 2013). Sample MJ20 is an exception, showing a temperature 10°C higher. This is probably due to the effect of greater borehole depth (Fig. 1B) and pressure. The Majnoon oilfield had the highest measured values (Table 1). Activity diagrams of Figures 5A and 5B show that Mg concentration in the brine seems to be limited by dolomite and by chlorite. To check the coexistence of the minerals, the thermodynamics of the following reaction have been calculated (Supplementary File 1):

$$CaMg(CO_3)_2 + 0.2\ Al_2Si_2O_5(OH)_4 + Ca^{2+} + 0.2\ SiO_2(aq) + 1.4\ H_2O =$$

$= 2\ H^+ + 0.2\ Mg_5Al_2Si_3O_{10}(OH)_8 + 2\ CaCO_3$

At P = 20 MPa and buffering conditions of Figure 5A, except for Mg which has been buffered by clinochlore, $Mg_5Al_2Si_3O_{10}(OH)_8$, instead of dolomite. The above reaction is in equilibria at 64°C using $\log[Ca^{2+}/(H^+)^2]$ = 11.11 and $\log[SiO_2(aq)]$ = -3.32, which corresponds to the mean activity values of all investigated samples (Supplementary File 1). Therefore, this corroborates not only that dolomite and chlorite could coexist in the studied basin, but also the temperature values obtained by geothermometers, in particular those by Li-Mg and chalcedony equations (Table 2).

Figure 5 also shows that the Ca/Na ratio is probably controlled by smectite instead of albite. The role of clays on the control of Na amount in solution by Ca-Na exchange or Na adsorption could also explain the lower temperatures of 42 ± 6 °C obtained using the Na/Li geothermometer (Kharaka and Mariner, 1989; Sanjuan et al., 2014) (Table 2). Similarly, the values obtained from the boron isotope geothermometer gave an underestimation of the brine temperature (Table 2). This could be due to a higher $\delta^{11}B$ value in Cretaceous seawater (up to 3‰ higher than the present; Lemarchand et al. 2002), together with a fractionation effect due to evaporation up to halite saturation (approximatively +4‰) (Vengosh et al. 1992). Actually, by subtracting a value of 7‰ from the original values of the brines, a mean temperature of 64 ± 6°C was obtained from the boron isotope geothermometric equation (Boschetti et al., 2015), which matches with that obtained by the calcite-dolomite-chlorite-kaolinite equilibria.

4.2. Oxygen and hydrogen stable isotope ratios

The isotope composition value — i.e. not considering the salt effect according to Horita et al. (1993) — of the studied formation water is similar to that of the Mishrif Formation values from the Qatar oilfield values (Danquigny et al., 2005) (Figure 6). However, the calculation of isotope activity due to the salt effect reveals a high enrichment in δ^2H (up to +8.3‰) and a

slight depletion in $\delta^{18}O$ (up to -0.3‰) in comparison to the analysed isotope composition. As presented in Figure 6, the isotope composition of the formation waters from the samples analyzed in this study fall close to the final part of the hook path derived from experimental seawater evaporation (e.g. Gonfiantini et al., 2018), thus confirming the marine origin of these samples, as previously inferred by the boron isotope (Awadh et al., 2018). It should be noted that the experimental hook paths of the evaporated seawater are generally analysed from salt pans without the addition of either new marine or meteoric water (i.e. closed system) (Gonfiantini, 1965; Gonfiantini et al., 2018). This could be the reason why the isotope activity values of the brine — i.e. considering the salt effect according to Horita et al. (1993) — do not fall on the hook path (Figure 6). In Figure 6, the Iraq meteoric water line (IMWL) and its prediction interval (parallel dashed lines with $\delta^{2}H \pm 10.3$ ‰ from IMWL) were recalculated from the rainwater isotope data of Ali et al. (2015) using the error-in-variable (EIV) regression method (Boschetti et al., 2019). The extrapolation of the best fit line of the brine samples meets the prediction interval of the meteoric water line just between rain waters collected from Baṣrah city (Fig. 1) plus other southern Iraq areas (Al-Kinani et al., 2018; Ali et al., 2015; Jassem et al., 2018) and evaporated river samples from the Tigris and Euphrates (Jassem et al., 2018) (Figure 6). Sample RU287 shows the highest contribution of modern fresh water. It should also be remarked that, in comparison with other samples, the RU287 brine displays barite supersaturation (Table 2), which is probably due to the effect of mixing between brines and local water of meteoric origin or reinjected produced waters as a consequence of the water flooding (Ghalib and Almallah, 2017; Sorbie and Mackay, 2000). This is in line with the previously described chemical diagrams. On the opposite side, the extrapolated best fit line of the isotope activity of the brines meets the hooked evaporation path of seawater just on the top of the hump (Figure 6), which approximatively corresponds to gypsum saturation (Holser, 1979; Knauth and Beeunas, 1986).

Evaporated seawater samples from present-day sabkha and lagoon environments (i.e. open systems) show $\delta^{18}O$ up to +6.5‰, which is similar to those determined in the formation brines of this study, but with $\delta^{2}H$ enrichment up to approximatively +30‰ (McKenzie et al., 1980; Nadler and Magaritz, 1980; Robinson and Gunatilaka, 1991). Lower deuterium values are mainly due to mixing with evaporated surface waters or groundwater of meteoric origin (McKenzie et al., 1980; Robinson and Gunatilaka, 1991); whereas, flooding and mixing of evaporated solution with new seawater inputs could shift the composition back to the starting values (i.e. near V-SMOW) (Nadler and Magaritz, 1980) (Figure 6). A similar effect was observed in Miocene brines by comparison with $\delta^{18}O$ from coeval gypsum, with the exception of the formation waters affected by a positive $\delta^{18}O$-shift as result of diagenetic water-rock interaction with limestones (Boschetti et al., 2011). In a similar way, and assuming that starting seawater during the Phanerozoic has remained isotopically similar to the present-day V-SMOW value (i.e. 0‰ both for oxygen and for hydrogen stable isotope ratios) (Gregory and Taylor Jr, 1981; Ryb and Eiler, 2018; Sessions, 2016), the ^{18}O enrichment of formation waters as observed in samples MJ20, ZB140, and R590 could be due to water–rock interaction. Therefore, water-rock interaction and dilution seem to be the main processes that affected in a significant manner the isotope composition of the studied brines.

Such a diagenetic effect was also hypothesised for the Mishrif Formation in Qatar where limestones value ranges between +24.4 ‰ < $\delta^{18}O$ (V-SMOW) < +27.4 ‰, formation brines $\delta^{18}O$ up to +5‰ (V-SMOW), and temperatures between 50 and 70°C have been measured (Deville de Periere, 2011). As the isotope values of the limestones from the same formation in southern Iraq are within the range of those measured in Qatar, i.e. +25.2 ‰ < $\delta^{18}O$ (V-SMOW) < +27.4 ‰ (Taha and Abdullah, 2019), the diagenetic effect can be hypothesised also for this area. Considering a mean value $\delta^{18}O(H_2O)a$ = +3.9 ‰ (V-SMOW) for the brine samples that fall within the diagenetic arrow in Figure 6 and a mean value of

$\delta^{18}O$ (limestones) equal to +26.5 ‰ (V-SMOW) of the Mishrif Formation in southern Iraq, it is possible to calculate an oxygen isotope fractionation factor of 1000lnα (calcite-water) = +22.3 ‰. This latter value corresponds to a temperature between 56°C (Kim and O'Neil, 1997) and 69°C (Zheng, 1999). Other isotope effects due to clays and crude are probably not quantitatively important or less pronounced than the salt effect. Indeed, a fractionation between water and hydrocarbons should generate in brines a shift towards $\delta^{2}H$ values higher than seawater (e.g., Horita, 2009), but this is not the case (Figure 6). Furthermore, the amount of clays minerals in the Mishrif Formation are probably insufficient to generate a significant isotope effect on the $\delta^{2}H$ of the waters.

4.3. Strontium isotope ratio

The strontium isotope ratios of the four brine samples analysed are $0.707713 < {}^{87}Sr/{}^{86}Sr < 0.707749$ (WQ87, RU287, ZB140, R590), which corresponds to a marine strontium of late Cenomanian–early Maastrichtian age (McArthur, 2010; McArthur et al., 2012); with the sample at the Majnoon oilfield (MJ20) showing the highest value of 0.708043. The Mishrif reservoir is Cenomanian–Turonian; therefore, the strontium isotope ratio should theoretically not be greater than 0.707314 ± 0.000005 (McArthur, 2010; McArthur et al., 2012). The higher strontium isotope ratios in formation waters could suggest a contribution of more radiogenic strontium from injected waters when compared to the more saline and enriched brines (Danquigny et al., 2005), but in this case the oxygen and hydrogen stable isotope ratios are not less than the other samples. Moreover, it should be also noted that $^{87}Sr/^{86}Sr$ values up to 0.707869 have been detected in the brines from the Mishrif Formation in Qatar (Al Khalij offshore field; Danquigny et al. 2005) and up to 0.70878 in the carbonate matrix of the coeval Sarvak Formation in southern Iran (Hajikazemi et al., 2012). Such elevated values detected at the disconformity surfaces of the formations are probably due to the contribution of meteoric water during diagenesis (e.g., Hajikazemi et al. 2012). However, the combination of high

manganese and radiogenic strontium contributions to the limestones of the Sarvak Formation of southern Iran were also attributed to different sources: i) a Cenomanian-Turonian subaerial exposure; ii) diagenetic fluids; and iii) detritus (Navidtalab et al., 2016). Actually, all the inspected brines of this study are undersatured with respect to pure rhodocrosite (SI = -3.9 ± 0.8), but in equilibrium with carbonate solid solution (SI = -0.082 ± 0.261) (Table 2). In particular, despite its high Mn activity, the Majnoon brine MJ20 showed a slight undersaturation in that solid solution. Therefore, the higher Mn concentration (up to 4 mg/l) and radiogenic strontium at that brine could be acquired by limestone dissolution in a disconformity layers. Alternatively, as suggested by the lowest gypsum and anhydrite saturation indices of the Majnoon sample (Table 2), it cannot be excluded that there was a contribution of radiogenic strontium-rich sulphate minerals from Cambrian salt domes (up to 0.7092) (McArthur et al., 2012). Salt domes characterise the fold settings in the oilfields of southern Iraq (Al-Ameri et al., 2011; Al-Mimar and Awadh, 2019). The doming triggered local uplift and emergence of paleo-exposure surfaces (Rahimpour-Bonab et al., 2013), thus the shallow back shoal/lagoonal depositional environment of Mishrif limestones at the Majnoon oilfield and the salt domes seem to be related (Aqrawi et al., 2010; Mahdi et al., 2013). Moreover, “hydrothermal fluids” with temperatures up to 80°C were hypothesized to form diagenetic cements (i.e., blocky calcite), dolomite and coarse crystalline pyrite during deeper burial of the Sarvak Formation (Hajikazemi et al., 2017). Therefore, the chemical, thermal and isotopic anomalies of the Majnoon brine suggest that it is the hottest fluid probably related to the higher geothermal gradient of a deeper structure as the ZFF (Basilici et al., 2020; Bordenave, 2008; Bordenave and Hegre, 2010).

5. Conclusions

This paper presented the first data on isotope ratios of oxygen, hydrogen, and strontium of oilfield waters from southern Iraq, along with new trace element data and a reinterpretation of

previous published chemistry. Processes like diagenesis and seawater evaporation that typically occur in these fluids can be distinguished using classical 'basinal fluid' chemical diagrams. Mishrif Formation waters are Cretaceous connate brines and the different chemical composition of seawater of that period needs to be taken into account for a more correct interpretation. The Ca-excess versus Na-deficit composition of these kinds of fluids are usually explained by albitisation. However, it was verified by activity plots that in the Mishrif limestone reservoir the Na/Ca exchange that occurs in brines is mainly due to water-smectite equilibrium.

The values $\delta^{2}H$ and $\delta^{18}O$ obtained on selected samples show that oxygen isotope composition of the brines was isotopically more affected by equilibria with limestone than evaporation. The global effect of the water-rock interaction is an ^{18}O-enrichment of the brines. Locally, dilution by present-day water of meteoric origin and shift towards the local meteoric water line also detected, probably as consequence of water-flooding (Rumaila South, sample RU287). Furthermore, it is also shown that isotope data cannot be separated from the interpretation of the chemical composition of sedimentary brines. The contribution of the salt effect on the stable isotope ratios of water molecules, i.e. $^{2}H/^{1}H$ and $^{18}O/^{16}O$, needs to be evaluated because this parameter could vary the results during fractionation processes such as seawater evaporation and diagenesis. Hydrogen isotope ratios are probably more affected by the salt effect than other fractionations. Furthermore, taking into account the salt effect, the temperature range inferred from carbonate-water oxygen isotope ratio fractionation is comparable to that obtained from the chemical geothermometers, i.e. between 50 and 75°C. According to Abeed et al. (2013), these evaluations confirm that the present-day borehole temperatures are not so different from those reached during Neogene burial.

More recent mixing processes such as water floods could be detected by a comparison with the composition of the formation brine, waters produced from crude dehydrators, and

the local waters of meteoric origin. The strontium isotope ratio confirms the interaction of Cretaceous limestone for most of the studied samples, suggesting a late Cenomanian–early Maastrichtian age, and an input of more radiogenic strontium in the Majnoon oilfield (MJ20 sample). The brine sample from this latter oilfield showed a particular geochemical characteristic. Despite the lower temperature measured at the MJ20 borehole (60°C), the slightly higher temperature obtained by the Li-Mg, Na-Li and $\delta^{11}B$ geothermometers (up to 74°C) is probably due to the deeper structure of that oilfield, which is closer to the ZFF. The more radiogenic strontium ratio at Majnoon could be related to: i) debris input in the limestone, which could explain also the high Mn content; or ii) interaction with local Cambrian sulphates. An inspection of additional samples, sulphur stable isotope ratio ($^{34}S/^{32}S$) and radiogenic isotope of the halogens (^{139}I, ^{36}Cl) could improve the knowledge of the past water flow events and clarify the relationship between the high Mn concentration / high radiogenic strontium in the Cretaceous limestones and the salt domes.

Acknowledgements

Special thanks to G. Venturelli for the comments and suggestions on a preliminary version of the manuscript. The authors very much appreciate the Associate Editor, B.J. Katz, and the two anonymous reviewers for their careful reading of the manuscript and all valuable constructive comments and suggestions.

Captions

Table 1 – Physicochemical parameters, major ion composition, trace elements concentration, and isotopic results from Awadh et al. (2018) and this study.

Table 2 – Geothermometric results in Celsius degree (°C); mineral saturation indices (SI), and carbon dioxide partial pressure as $logP(CO_2)g$ obtained by PHREECI code, version 3, along with Pitzer thermodynamic dataset at the measured temperature and water pressure conditions (Table 1). EQ 3/6 code was also used to calculate the saturation indexes of carbonates solid solution.

Figure 1 **–** A) Location map showing the studied oilfields at the Zubair zone, within the southern part of the Mesopotamia plain and to the southwest of the Zagros Foredeep Fault (ZFF); Stratigraphic correlation of the five oilfield wells penetrating four formations

(Rumaila, Mishrif, Khasib, and Tanuma) in which there is a well from each oilfield (RU287 from Rumaila South, R590 from Rumaila North, WQ87 from West Qurna, MJ20 from Majnoon, and ZB140 from Zubair oilfield); B) Typical section represents the stratigraphic setting in the study area.

Figure 2 **–** Langelier–Ludwig (A) and Brine Differentiation Plot (B) of the oilfield brines of southern Iraq (Al-Mallah, 2014; Al-Marsoumi and Abdul-Wahab, 2005; Awadh et al., 2019b; Awadh et al., 2018; Jamil, 1978) compared with shallow groundwater (Hamdan, 2017), Shatt Al-Arab River (ROPME, 2011), Shatt Al-Basrah Canal, or 'Main Drain' (Al-Mallah, 2014) and seawater. In both diagrams, concentration of the dissolved species are in equivalent/liter; dashed ellipses depict the trend of the Tigris–Euphrates River system at Qurna and Shatt Al-Arab River during the 60s (Rzóska, 1980). In (B), Mishrif Formation's brine waters from Awadh et al. (2018) are distinguished by black triangles; the five samples reprised in this study are highlighted by white crosses. The brine data from other references (Al-Mallah, 2014; Al-Marsoumi and Abdul-Wahab, 2005; Awadh et al., 2019b; Jamil, 1978) are represented by white triangles. Produced waters from hydrocarbon dehydrators are also shown for comparison (dashed field) (Al-Furaiji, 2016; Al-Shamkhani, 2013). Arrows depict possible mixing trends. In the inset, the original fields of the diagram along with evaporation paths of present-day (Boschetti, 2011; Hounslow, 1995) and Cretaceous seawater (this study) are shown. G and H depict the gypsum and halite saturation points, respectively.

Figure 3 **–** Ca-excess = 2 x $[Ca_{meas} - (Ca/Cl)_{SW} \times Cl_{meas}]/40.08$ vs. Na-defict = $[(Na/Cl)_{SW} \times Cl_{meas} - Na_{meas}] / 22.99$ diagram for oilfield waters from southern Iraq, where meas = measured, SW = seawater and Ca, Na and Cl are elemental concentrations in mg/l (Davisson and Criss, 1996). The 1Ca-2Na or 1Ca-1Na exchange arrows depict the possible paths of formation fluids in sedimentary basins during plagiocalse albitisation (Davisson and Criss, 1996). In (A) and (B) diagrams, present-day and Cretaceous seawater were used as SW-composition, respectively. In both: light gray ellipse at the origin of the plot represents the initial seawater composition (i.e. before evaporation), local groundwater and surface waters composition; dashed and dot-dashed lines depict the evaporation paths of Cretaceous and present-day seawaters, respectively. Other symbols and fields as in Figure 2.

Figure 4 **–** Base-10 logarithm of silicium versus calcium/magnesium ratio diagram of the Mishrif Formation's brines from southern Iraq (molar concentration). Dashed curves depict the simultaneous equilibria of calcite-dolomites plus quarz (light gray) or chacedony (black) calculated by PHREEQCI code and pitzer thermodynamic dataset (Parkhurst and Appelo, 2013) at the mean pressure of the five samples (27.8 MPa; Table 1).

Figure 5 **–** Activity plots for the system Na_2O-CaO-MgO-Al_2O_3-SiO_2-H_2O-CO_2 at P = 200 bar and 50 < T < 75 °C. In (A), the activity of dissolved silica has been fixed at the mean value detected in the waters, i.e.: $\log[SiO_2(aq)] = -3.32$, whereas in (B) it was buffered by chalcedony. In both diagrams: water activity at $\log[H_2O] = -0.0855$ (mean value of the local brines); aluminium buffered by kaolinite; magnesium and HCO_3^- buffered by dolomite and calcite, respectively.

Figure 6 **–** $\delta^2H(H_2O)$ vs. $\delta^{18}O(H_2O)$ diagram. Samples from this study are diffentiated for isotope composition (white-crossed gray triangles) and isotope activity (white-crossed black triangles): the former represent analytical results of water samples after vacuum distillation and IRMS; the latter represent isotope composition plus the theoretical salt effect (Horita et al., 1993) (Table 1). Water isotope composition of brines from the Mishrif Formation in Qatar are also shown for comparison (open triangles) (Danquigny et al., 2005). Dotted lines depict the linear best fits of the two ways of representation of isotope ratios in brines.

Evaporated seawaters from a closed (Gonfiantini et al., 2018) and open (McKenzie et al., 1980; Nadler and Magaritz, 1980; Robinson and Gunatilaka, 1991) system are shown for comparison. The previous published data on isotope composition of the Arabian Gulf seawater and its evaporated composition are depicted by the field with waves and forward-back curved arrows, respectively (Bagheri et al., 2014; McKenzie et al., 1980; Robinson and Gunatilaka, 1991; Yurtsever, 1994). Rainwater samples (drops) from southern Iraq (Al-Kinani et al., 2018; Ali et al., 2015; Jassem et al., 2018) and nothern Kuwait (Hadi et al., 2016) are also shown for comparison. Tigris and Euphrates samples are represented by open squares; samples out of the IMWL's (Iraq meteoric water line) prediction interval are evaporated surface water samples (arrow with slope ~ 4.3) (Ali et al., 2015; Jassem et al., 2018).

Supplementary File 1 - Calculation of the thermodynamic equilibria by Rxn tool of The Geochemist's Workbench® code (Bethke and Yeakel, 2008) and P = 20 MPa thermodynamic dataset (Boschetti et al., 2016). To reduce the variables, the activity of calcium and hydrogen was rewritten as log-ratio in the reaction and automatically rebalanced by the tool.

References

Abbas, L.K., Mahdi, T.A., 2019. Reservoir units of Mishrif Formation in Majnoon Oil field, Southern Iraq. Iraqi Journal of Science 60, 2656-2663.

Abeed, Q., Leythaeuser, D., Littke, R., 2012. Geochemistry, origin and correlation of crude oils in Lower Cretaceous sedimentary sequences of the southern Mesopotamian Basin, southern Iraq. Organic Gechemistry 46, 113-126.

Abeed, Q., Littke, R., Strozyk, F., Uffmann, A.K., 2013. The Upper Jurassic–Cretaceous petroleum system of southern Iraq: A 3-D basin modelling study. GeoArabia 18, 179-200.

Al-Ameri, T.K., Jafar, M.S., Pitman, J., 2011. Hydrocarbon generation modeling of the Basrah oil fields, Southern Iraq. University of Baghdad, Jadiriyah, AAPG Annual Convention and Exhibition. AAPG Search and Discovery, Houston, Texas.

Al-Furaiji, M., 2016. Hyper-saline produced water treatment for beneficial use. University of Twente, Gildeprint - The Netherlands.

Al-Kinani, S.A.A., Falih, A.H., Al-abidin, H.A.Z., Al-Naseri, S.K.A.A.H., 2018. Determination of the Meteoric Water Line Using Stable Isotopes in Precipitations at Several Locations In Baghdad. Iraqi Journal of Science and Technology 4, 36-42.

Al-Mallah, I.A., 2014. Assessment of the Environmental, Hydrological and Hydrogeological changes of the Main Drain, Iraq, College of Science - Department of Geology. University of Basrah, Basrah, Iraq.

Al-Marsoumi, A.M.H., Abdul-Wahab, D.S., 2005. Hydrogeochemistry of Yamama Reservoir formation water - west Qurna oil field - Southern Iraq. Basrah Journal of Science 23, 10-20.

Al-Mimar, H.S., Awadh, S.M., 2019. The Role of Chemistry of the Oil-Field Water in the Distribution of Reservoir Pressures: A Case Study of Mishrif Reservoir in the Southern Oil-Fields, Iraq. Journal of Petroleum Research & Studies 22, E52-E64.

Al-Mimar, H.S., Awadh, S.M., Al-Yaseri, A.A., Yaseen, Z.M., 2018. Sedimentary units-layering system and depositional model of the carbonate Mishrif reservoir in Rumaila oilfield, Southern Iraq. Modeling Earth Systems and Environment 4, 1449-1465.

Al-Shamkhani, M.T., 2013. Managing, Controlling and Improving the Treatment of Produced Water Using the Six Sigma Methodology for the Iraqi Oil Fields, College of Engineering and Computer Science - Department of Industrial Engineering and Management Systems. University of Central Florida, Orlando, Florida.

Al-Ziayyir, H.G.F., 2018. Mineralisation-Related Flow Heterogeneity within the Zubair Formation in the Rumaila Oilfield, Southern Iraq, Faculty of Science and Engineering. University of Manchester, Manchester.

Ali, K.K., Al-Kubaisi, Q.Y., Al-Paruany, K.B., 2015. Isotopic study of water resources in a semi-arid region, western Iraq. Environmental Earth Sciences 74, 1671-1686.

Alsharhan, A.S., Nairn, A.E.M., 1988. A review of the Cretaceous Formations in the Arabian Peninsula and Gulf: Part II. Mid-Cretacous (Wasia Group) Stratigraphy and Paleogeography. Journal of Petroleum Geology 11, 89-112.

Alyasi, A.I., Al-Jawad, S.N., Alshabender, L.Y., 2014. Geophysical Study to the Role of Salt in Creating Buzurgan Oilfield Structure, Southeast of Iraq. Iraqi Journal of Science 55, 1579-1587.

Aqrawi, A.A.M., Horbury , A.D., Sadooni, F.N., Goff, J.C., 2010. The Petroleum Geology of Iraq. Scientific Press, Beaconsfield, Bucks, UK.

Aqrawi, A.A.M., Thehni, G.A., Sherwani, G.H., Kareem, B.M.A., 1998. Mid-Cretaceous rudist-bearing carbonates of the Mishrif Formation: an important reservoir sequence in the Mesopotamian Basin, Iraq. Journal of Petroleum Geology 21, 57-82.

Awadeesian, A.M., Awadh, S.M., Al-Dabbas, M.A., Al-Maliki, M.M., Al-Jawad, S.N., Hussein, A.K.S., 2019. A modified water injection technique to improve oil recovery: Mishrif carbonate resevoirs in Southern Iraq oil fileds, case study. Iraqi Geological Journal 52, 125-146.

Awadh, S., Al-Mimar, H., Al-yaseri, A., 2019a. Potentiometric Salinity Mapping of Mishrif Oilfield Waters in (Iraq's) Southern Oil Fields, in: Chaminé, H.I., Barbieri, M., Kisi, O., Chen, M., Merkel, B.D. (Eds.), Advances in Sustainable and Environmental Hydrology, Hydrogeology, Hydrochemistry and Water Resources - Proceedings of the 1st Springer

Conference of the Arabian Journal of Geosciences (CAJG-1), Tunisia 2018. Springer Nature, Switzerland, pp. 49-52.

Awadh, S.M., Al-Auweidy, M.R., Al-Yaseri, A.A., 2019b. Hydrochemistry as a tool for interpreting brine origin and chemical equilibrium in oilfields: Zubair reservoir southern Iraq case study. Applied Water Science, 93.

Awadh, S.M., Al-Mimar, H.S., Al-Yaseri, A.A., 2018. Salinity mapping model and brine chemistry of Mishrif reservoir in Basrah oilfields, Southern Iraq. Arabian Journal of Geosciences 11.

Bąbel, M., Schreiber, B.C., 2014. Geochemistry of Evaporites and Evolution of Seawater in: Holland, H.D., Turekian, K.K. (Eds.), Treatise on Geochemistry, 2nd ed. Elsevier, Printed and bound in Italy, pp. 483-560.

Bagheri, R., Nadri, A., Raeisi, E., Eggenkamp, H.G.M., Kazemi, G.A., Montaseri, A., 2014. Hydrochemical and isotopic ($\delta^{18}O$, $\delta^{2}H$, $^{87}Sr/^{86}Sr$, $\delta^{37}Cl$ and $\delta^{81}Br$) evidence for the origin of saline formation water in a gas reservoir. Chemical Geology 384, 62-75.

Basilici, M., Mazzoli, S., Megna, A., Santini, S., Tavani, S., 2020. 3-D Geothermal Model of the Lurestan Sector of the Zagros Thrust Belt, Iran. Energies 13.

Bethke, C.M., Yeakel, S., 2008. The Geochemist's Workbench® - Release 7. GWB Essentials Guide, Hydrogeology Program. University of Illinois.

Bordenave, M.L., 2008. The origin of the Permo-Triassic gas accumulations in the Iranian Zagros foldbelt and contiguous offshore areas: a review of the Palaeozoic petroleum system. Journal of Petroleum Geology 31, 3-42.

Bordenave, M.L., Hegre, J.A., 2010. Current distribution of oil and gas fields in the Zagros Fold Belt of Iran and contiguous offshore as the result of the petroleum systems, in: Leturmy, P., Robin, C. (Eds.), Tectonic and Stratigraphic Evolution of Zagros and Makran during the Mesozoic–Cenozoic. The Geological Society of London, London, pp. 291-353.

Boschetti, T., 2011. Application of brine differentiation and Langelier–Ludwig plots to fresh-to-brine waters from sedimentary basins: Diagnostic potentials and limits. Journal of Geochemical Exploration, 108, 126-130.

Boschetti, T., Angulo, B., Cabrera, F., Vásquez, J., Montero, R.L., 2016. Hydrogeochemical characterization of oilfield waters from southeast Maracaibo Basin (Venezuela): Diagenetic effects on chemical and isotopic composition. Marine and Petroleum Geology 73, 228-248.

Boschetti, T., Cifuentes, J., Iacumin, P., Selmo, E., 2019. Local Meteoric Water Line of Northern Chile (18°S - 30°S): An application of error-in-variables regression to the oxygen and hydrogen stable isotope ratio of precipitation. Water 11

Boschetti, T., Toscani, L., Salvioli Mariani, E., 2015. Boron isotope geochemistry of Na- bicarbonate, Na- chloride, and Ca- chloride waters from the Northern Apennine Foredeep basin: other pieces of the sedimentary basin puzzle. Geofluids 15, 546-562.

Boschetti, T., Toscani, L., Shouakar-Stash, O., Iacumin, P., Venturelli, G., Mucchino, C., Frape, S.K., 2011. Salt waters of the Northern Apennine Foredeep Basin (Italy): origin and evolution. Aquatic Geochemistry 17, 71-108.

Clesceri, L.S., Greenberg, A.E., Eaton, A.D., 1999. Method 4500-SiO_2 D, Heteropoly Blue Method, Standard methods for the examination of water and wastewater, 20th. American Public Health Association, American Water Works Association, Water Environment Federation, Washington.

Danquigny, J.A., Matthews, J., Noman, R., Mohsen, A., 2005. Assessment of interwell communication in the carbonate Al Khalij oil field using isotope ratio water sample analysis, International Petroleum Technology Conference. IPTC, Doha, Qatar

Davisson, M.L., Criss, R.E., 1996. Na-Ca-Cl relations in basinal fluids. Geochimica et Cosmochimica Acta 60, 2743-2752.

Deville de Periere, M., 2011. Origine sédimento-diagénétique de réservoirs carbonatés microporeux: exemple de la formation Mishrif (Cénomanien) du Moyen-Orient. Université de Bourgogne.

Ghalib, H.B., Almallah, I.A.R., 2017. Scaling simulation resulting from mixing predicted model between Mishrif formation water and different waters injection in Basrah oil field, southern Iraq. Modeling Earth Systems and Environment 3, 1557-1569.

Giggenbach, W.F., 1991. Chemical Techniques in geothermal exploration, in: D'Amore, F. (Ed.), Application of Geochemistry in Geothermal Reservoir Development. UNITAR, Rome, Italy, pp. 119–144.

Gonfiantini, R., 1965. Effetti isotopi nell'evaporazione di acque salate. Atti della Società Toscana di Scienze Naturali - Memorie, Serie A 72, 1-22.

Gonfiantini, R., Wassenaar, L.I., Araguas-Araguas, L., Aggarwal, P.K., 2018. A unified Craig-Gordon isotope model of stable hydrogen and oxygen isotope fractionation during fresh or saltwater evaporation. Geochimica et Cosmochimica Acta 235, 224-236.

Grabowski Jr., G.J., 2014. Iraq, in: Marlow, L., Kendall, M.C., Yose, L.A. (Eds.), Petroleum systems of the Tethyan region. The American Association of Petroleum Geologists, Tulsa, OK U.S.A., pp. 379–467.

Gregory, R.T., Taylor Jr, H.P., 1981. An oxygen isotope profile in a section of Cretaceous oceanic crust, Samail Ophiolite, Oman: Evidence for $\delta^{18}O$ buffering of the oceans by deep (>

5 km) seawater- hydrothermal circulation at mid- ocean ridges. Journal of Geophysical Research: Solid Earth 86, 2737-2755.

Hadi, K., Kumar, U.S., Al-Senafy, M., Bhandary, H., 2016. Environmental isotope systematics of the groundwater system of southern Kuwait. Environmental Earth Sciences 75.

Hajikazemi, E., Al-Aasm, I.S., Coniglio, M., 2017. Diagenetic history and reservoir properties of the Cenomanian-Turonian carbonates in southwestern Iran and the Persian Gulf. Marine and Petroleum Geology 88, 845-857.

Hajikazemi, E., Al- Aasm, I.S., Coniglio, M., 2012. Chemostratigraphy of Cenomanian–Turonian carbonates of the Sarvak Formation, southern Iran. Journal of Petroleum Geology 35, 187-205.

Hamdan, A.N.A., 2017. The use of water quality index to evaluate groundwater quality in west of Basrah wells. Kufa Journal of Engineering 8, 51-64.

Holser, W., 1979. Trace elements and isotopes in evaporites, in: Burns, R.G. (Ed.), Marine Minerals. De Gruyter - Mineralogical Society of America, Berlin, Boston, pp. 295–346.

Hönisch, B., Ridgwell, A., Schmidt, D.N., Thomas, E., Gibbs, S.J., Sluijs, A., Zeebe, R., Kump, L., Martindale, R.C., Greene, S.E., Kiessling, W., Ries, J., Zachos, J.C., Royer, D.L., Barker, S., Marchitto Jr., T.M., Moyer, R., Pelejero, C., Ziveri, P., Foster, G.L., Williams, B., 2012. The geological record of ocean acidification. Science 335, 1058-1063.

Horita, J., 2009. Isotopic evolution of saline lakes in the low-latitude and polar regions. Aquatic Geochemistry 15, 43-69.

Horita, J., Cole, D.R., Wesolowski, D.J., 1993. The activity-composition relationship of oxygen and hydrogen isotopes in aqueous salt solutions: II. Vapor-liquid water equilibration of mixed salt solutions from 50 to 100 C and geochemical implications. Geochimica et Cosmochimica Acta 57, 4703-4711.

Hounslow, A.W., 1995. Water Quality Data Analysis and Interpretation. Lewis Publishers, Boca Raton, New York.

Jamil, A.K., 1978. Hydrochemical and Hydrodynamic Zones and the Probable Direction of Water Flow within Zubair Reservoir of Zubair and Rumaila Oil Fields (Southern Iraq). Geologisches Jahrbuch, Reihe D, D25, 199-211.

Jassem, A.A., Nada, K.B., Abdualamer, Z.S., 2018. Using ^{18}O, ^{2}H isotopes to study the effect of fish lake on sueface water in Al-Azezeya, Kut Governatorate, Iraq. The Iraqi Geological Journal 51, 149-156.

Jassim, S.Z., Buday, T., 2006. Units of the Stable Shelf, in: Jassim, S.Z., Goff, J.C. (Eds.), Geology of Iraq. Dolin, Prague and Moravian Museum, Brno. Czech Republic, pp. 53-72.

Kharaka, Y.K., Mariner, R.H., 1989. Chemical geothermometers and their application to formation waters from sedimentary basins, in: Naeser, N.D., McCollin, T.H. (Eds.), Thermal history of sedimentary basins. Springer-Verlag, New York, pp. 99–117.

Kim, S.T., O'Neil, J.R., 1997. Equilibrium and nonequilibrium oxygen isotope effects in synthetic carbonates. 61 Geochimica et cosmochimica acta, 3461-3475.

Knauth, L.P., Beeunas, M.A., 1986. Isotope geochemistry of fluid inclusions in Permian halite with implications for the isotopic history of ocean water and the origin of saline formation waters. Geochimica et Cosmochimica Acta 50, 419-433.

Konyuhov, A.I., Maleki, B., 2006. The Persian Gulf Basin: Geological history, sedimentary formations, and petroleum potential. Lithology and Mineral Resources 41, 344–361

Lemarchand, D., Gaillardet, J., Lewin, E., Allegre, C.J., 2002. Boron isotope systematics in large rivers: implications for the marine boron budget and paleo-pH reconstruction over the Cenozoic. Chemical Geology 190, 123-140.

Lowenstein, T.K., Hardie, L.A., Timofeeff, M.N., Demicco, R.V., 2003. Secular variation in seawater chemistry and the origin of calcium chloride basinal brines. Geology 31, 857-860.

Mahdi, T.A., Aqrawi, A.A., Horbury, A.D., Sherwani, G.H., 2013. Sedimentological characterization of the mid-Cretaceous Mishrif reservoir in southern Mesopotamian Basin, Iraq. GeoArabia 18, 139-174.

McArthur, J.M., 2010. Strontium isotope stratigraphy, in: Ratcliffe, K.T., Zaitlin, B.A. (Eds.), Application of modern stratigraphic techniques: theory and case histories. SEPM Society for Sedimentary Geology, Tulsa, Oklahoma, pp. 129–142.

McArthur, J.M., Howarth, R.J., Shields, G.A., 2012. Strontium isotope stratigraphy, in: Gradstein, F.M., Ogg, J.G., Schmitz, M.D., Ogg, G.M. (Eds.), The geologic time scale 2012. Elsevier, Oxford, pp. 127–144.

McKenzie, J.A., Hsü, K.J., Schneider, J.F., 1980. Movement of subsurface waters under the sabkha Abu Dhabi, UAE, and its relation to evaporative dolomite genesis, in: Zenger, D.H., Dunham, J.B., Ethington, R.L. (Eds.), Concepts and Models of Dolomitization. SEPM Society for Sedimentary Geology, Tulsa, Oklahoma, USA, pp. 11-30.

Mortazavi, M., Heuss-Assbichler, S., Shahri, M., 2017. Hydrothermal systems in the salt domes of south Iran. Procedia Earth and Planetary Science 17, 913-916.

Murris, R.J., 1980. Middle East: stratigraphic evolution and oil habitat. AAPG Bulletin 64, 597-618.

Nadler, A., Magaritz, M., 1980. Studies of marine solution basins isotopic and compositional changes during evaporation, in: Nissembaum, A. (Ed.), Hypersaline Brines and Evaporitic Environments. Elsevier, Amsterdam, The Netherlands, pp. 115-129.

Navidtalab, A., Rahimpour-Bonab, H., Huck, S., Heimhofer, U., 2016. Elemental geochemistry and strontium-isotope stratigraphy of Cenomanian to Santonian neritic carbonates in the Zagros Basin, Iran. Sedimentary Geology 346, 35-48.

Parkhurst, D.L., Appelo, C.A.J., 2013. Description of input and examples for PHREEQC version 3: a computer program for speciation, batch-reaction, one-dimensional transport, and inverse geochemical calculations Techniques and Methods. US Geological Survey, Reston, VA, p. This report is Chapter 43 of Section A: Groundwater in Book 46 Modeling Techniques.

Rahimpour- Bonab, H., Mehrabi, H., Navidtalab, A., Omidvar, M., Enayati- Bidgoli, A.H., Sonei, R., Sajjadi, F., Amiri-Bakhtyar, H., Arzani, N., Izadi- Mazidi, E., 2013. Palaeo- exposure surfaces in Cenomanian–santonian carbonate reservoirs in the Dezful embayment, SW Iran. Journal of Petroleum Geology 36, 335-362.

Robinson, B.W., Gunatilaka, A., 1991. Stable isotope studies and the hydrological regime of sabkhas in southern Kuwait, Arabian Gulf. Sedimentary Geology 73, 141-159.

ROPME, 2011. The Marshes-Shatt al-Arab- Gulf System, in: Environment, R.O.f.t.P.o.t.M. (Ed.). Marine Science Centre – University of Basra in Cooperation with Ministry of Environment Iraq, p. 102.

Rosenthal, E., 1997. Thermomineral waters of Ca-chloride composition: review of diagnostics and of brine evolution. Environmental Geology 32, 245-250.

Ryb, U., Eiler, J.M., 2018. Oxygen isotope composition of the Phanerozoic ocean and a possible solution to the dolomite problem. Proceedings of the National Academy of Sciences 115, 6602-6607.

Rzóska, J., 1980. Euphrates and Tigris, Mesopotamian ecology and destiny. Dr. W. Junk bv Publishers, The Hague The Netherlands.

Sadooni, F.N., 2005. The nature and origin of Upper Cretaceous basin-margin rudist buildups of the Mesopotamian Basin, southern Iraq, with consideration of possible hydrocarbon stratigraphic entrapment. Cretaceous Research 26, 213-224.

Sadooni, F.N., Aqrawi, A.A.M., 2000. Cretaceous sequence stratigraphic and petroleum potential of the Mesopotamian basin, Iraq, in: Alsharhan, A.S., Scott, R.W. (Eds.), Middle East Models of Jurassic/Cretaceous Carbonate Systems. SEPM Society for Sedimentary Geology, Tulsa, Oklahoma, USA, pp. 315-334.

Sanjuan, B., Millot, R., Asmundsson, R., Brach, M., Giroud, N., 2014. Use of two new Na/Li geothermometric relationships for geothermal fluids in volcanic environments. Chemical Geology 389, 60-81.

Sessions, A.L., 2016. Factors controlling the deuterium contents of sedimentary hydrocarbons. Organic Geochemistry 96, 43–64.

Singh, P., 2012. New Insights to the Implications of Salt Tectonics in the Northern Part of Kuwait Arch: An Integrated Modeling Study, First EAGE Workshop on Iraq-Hydrocarbon Exploration and Field Development. European Association of Geoscientists & Engineers (EAGE), Istanbul, Turkey

Sissakian, V., Abdul Ahad, A., Al-Ansari, N., Knutsson, S., 2017. Geomorphology, Geology and Tectonics of Jabal Sanam, Southern Iraq. Journal of Earth Sciences and Geotechnical Engineering 7, 97-113.

Sorbie, K.S., Mackay, E.J., 2000. Mixing of injected, connate and aquifer brines in waterflooding and its relevance to oilfield scaling. Journal of Petroleum Science and Engineering. 27, 85-106.

Taha, T.M., Abdullah, E.J., 2019. Reconstruction of Paleo depth and Paleo temperature from C-O stable isotope records of Mishrif Formation, southern Iraq. Iraqi Journal of Science 60, 1730-1742.

Vengosh, A., Starinsky, A., Kolodny, Y., Chivas, A.R., Raab, M., 1992. Boron isotope variations during fractional evaporation of sea water: new constraints on the marine vs. nonmarine debate. Geology 20, 799–802.

Wang, Y., Huang, C., Sun, B., Quan, C., Wu, J., Lin, Z., 2014. Paleo-CO_2 variation trends and the Cretaceous greenhouse climate. Earth-Science Reviews 129, 136-147.

Wolery, T.W., Jarek, R.L., 2003. EQ3/6, version 8.0—software user's manual. Civilian radioactive waste management system, Management & Operating Contractor, Sandia National Laboratories, Albuquerque, New Mexico.

Yurtsever, Y., 1994. Role of environmental isotopes in studies related to salinization processes and salt water intrusion dynamics, 13th Salt Water Intrusion Meeting - Session 3: Hydrogeochemical and environmental isotope studies. Mixing zone. Characterization of the origin and dynamics of salt and brackish waters, Cagliari, Italy, pp. 5-10.

Zheng, Y.-F., 1999. Oxygen isotope fractionation in carbonate and sulfate minerals. Geochemical Journal 33, 109-126.

Figure

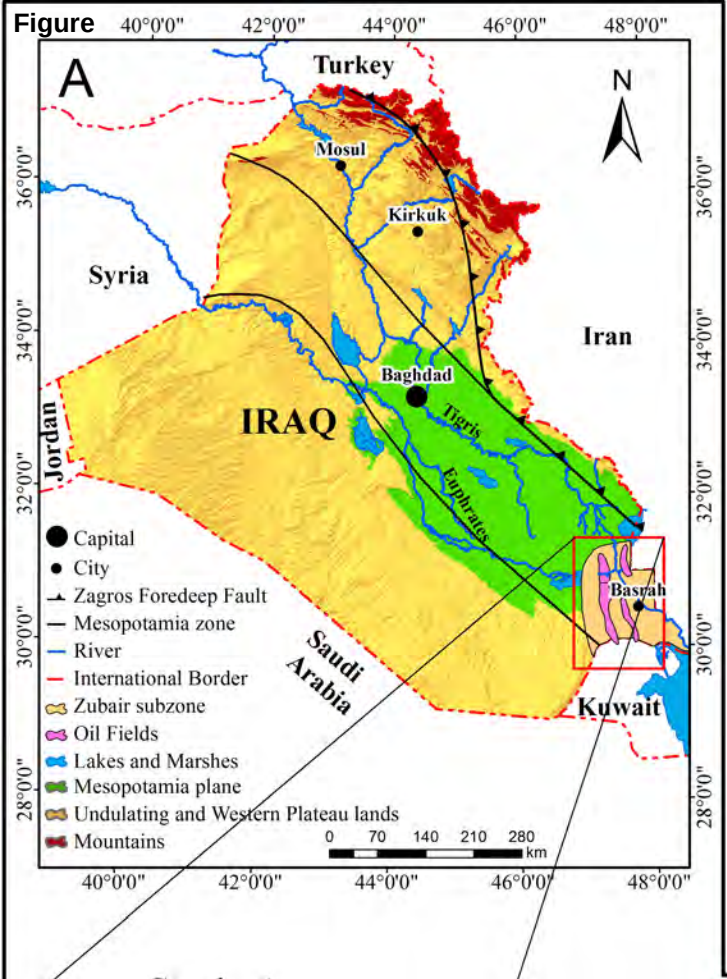
A
Turkey
Mosul
Kirkuk
Syria
Iran
Baghdad
IRAQ
Jordan
Tigris
Euphrates
Basrah
Saudi Arabia
Kuwait
N
Capital
City
Zagros Foredeep Fault
Mesopotamia zone
River
International Border
Zubair subzone
Oil Fields
Lakes and Marshes
Mesopotamia plane
Undulating and Western Plateau lands
Mountains
0 70 140 210 280 km
40°0'0" 42°0'0" 44°0'0" 46°0'0" 48°0'0"
36°0'0" 34°0'0" 32°0'0" 30°0'0" 28°0'0"

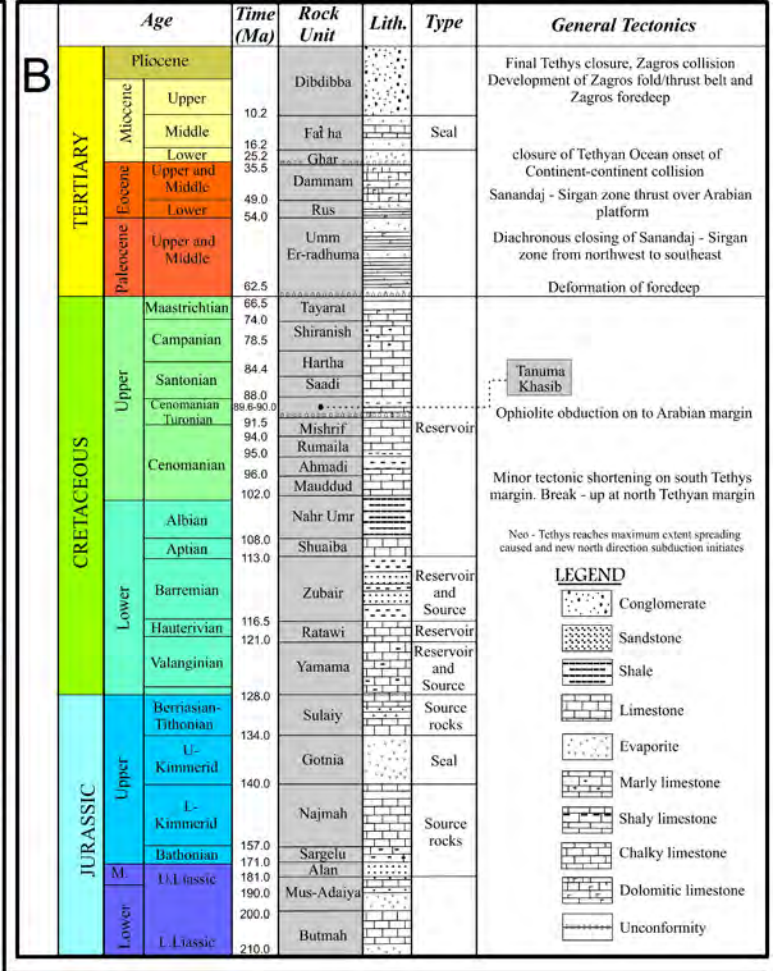
B
Age
Time (Ma)
Rock Unit
Lith.
Type
General Tectonics
TERTIARY
Pliocene
Miocene
Upper
Middle
Lower
Eocene
Upper and Middle
Lower
Paleocene
Upper and Middle
Dibdibba
Fat'ha
Ghar
Dammam
Rus
Umm Er-radhuma
Seal
Final Tethys closure, Zagros collision
Development of Zagros fold/thrust belt and Zagros foredeep
closure of Tethyan Ocean onset of Continent-continent collision
Sanandaj - Sirgan zone thrust over Arabian platform
Diachronous closing of Sanandaj - Sirgan zone from northwest to southeast
Deformation of foredeep
CRETACEOUS
Upper
Maastrichtian
Campanian
Santonian
Cenomanian
Turonian
Cenomanian
Lower
Albian
Aptian
Barremian
Hauterivian
Valanginian
Tayarat
Shiranish
Hartha
Saadi
Mishrif
Rumaila
Ahmadi
Mauddud
Nahr Umr
Shuaiba
Zubair
Ratawi
Yamama
Reservoir
Tanuma Khasib
Ophiolite obduction on to Arabian margin
Minor tectonic shortening on south Tethys margin. Break - up at north Tethyan margin
Neo - Tethys reaches maximum extent spreading caused and new north direction subduction initiates
Reservoir and Source
Reservoir
Reservoir and Source
JURASSIC
Upper
Berriasian-Tithonian
U. Kimmerid
L. Kimmerid
Bathonian
M.
U. Liassic
Lower
L. Liassic
Sulaiy
Gotnia
Najmah
Sargelu
Alan
Mus-Adaiya
Butmah
Source rocks
Seal
Source rocks
LEGEND
Conglomerate
Sandstone
Shale
Limestone
Evaporite
Marly limestone
Shaly limestone
Chalky limestone
Dolomitic limestone
Unconformity

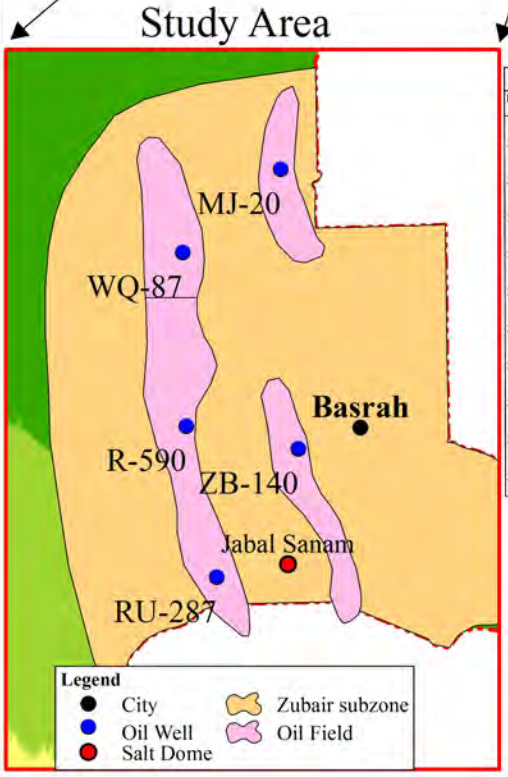
Study Area
MJ-20
WQ-87
Basrah
R-590
ZB-140
Jabal Sanam
RU-287
Legend
City
Oil Well
Salt Dome
Zubair subzone
Oil Field

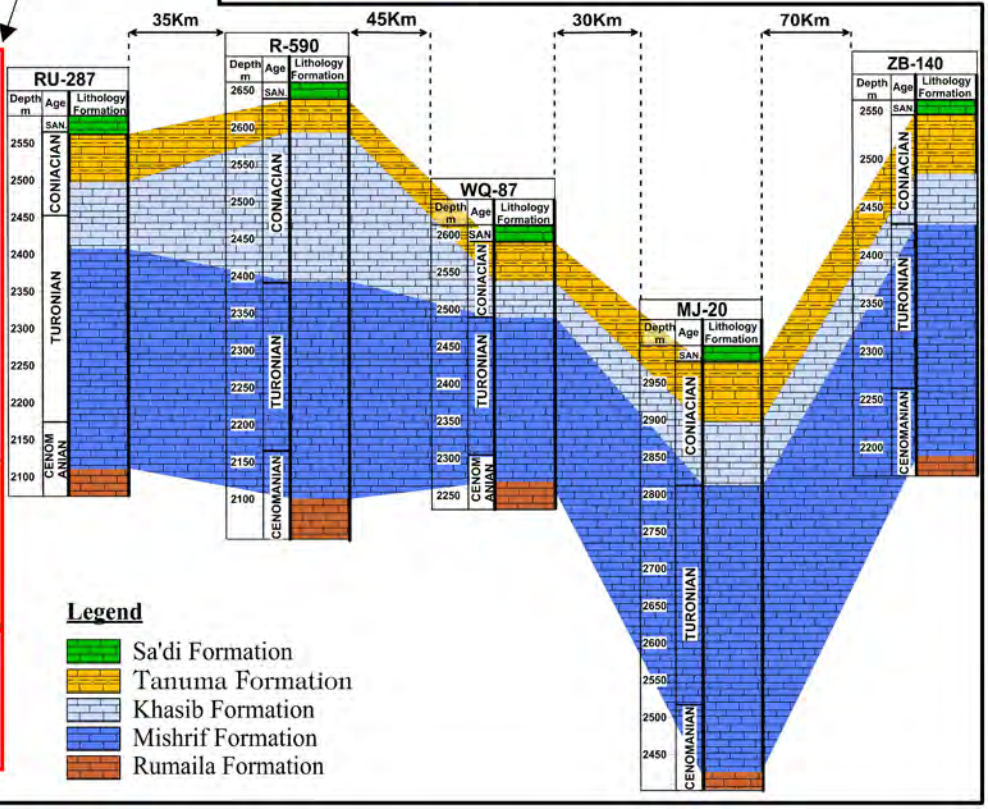
35Km
45Km
30Km
70Km
RU-287
R-590
WQ-87
MJ-20
ZB-140
Depth m
Age
Lithology Formation
SAN.
CONIACIAN
TURONIAN
CENOMANIAN
Legend
Sa'di Formation
Tanuma Formation
Khasib Formation
Mishrif Formation
Rumaila Formation

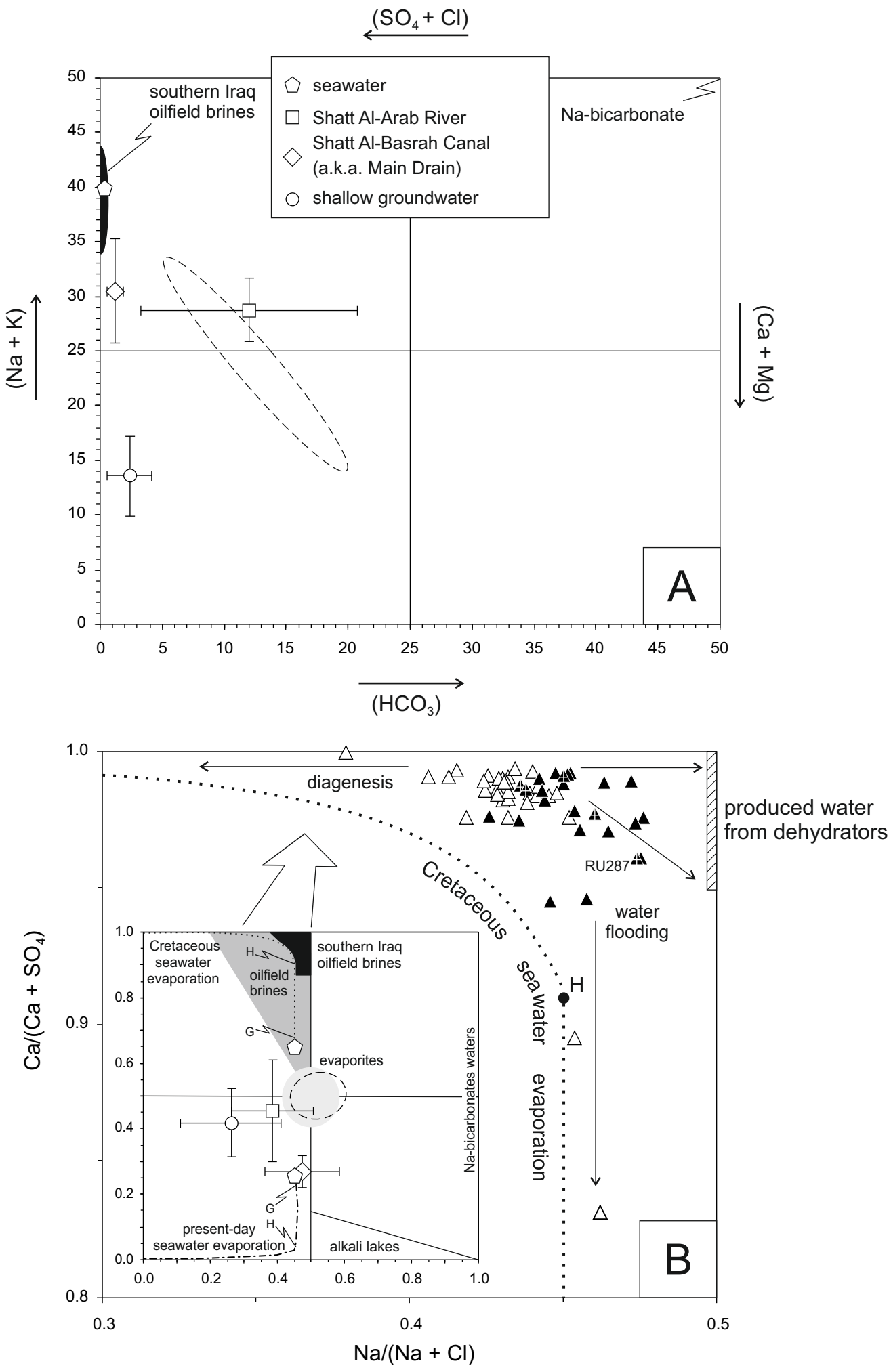
(SO4 + Cl)
seawater
Shatt Al-Arab River
Shatt Al-Basrah Canal
(a.k.a. Main Drain)
shallow groundwater
southern Iraq
oilfield brines
Na-bicarbonate
(Na + K)
(Ca + Mg)
(HCO3)
A
diagenesis
produced water
from dehydrators
RU287
Cretaceous
water
flooding
seawater evaporation
H
Ca/(Ca + SO4)
Na/(Na + Cl)
Cretaceous
seawater
evaporation
oilfield
brines
southern Iraq
oilfield brines
G
evaporites
Na-bicarbonates waters
present-day
seawater evaporation
alkali lakes
B

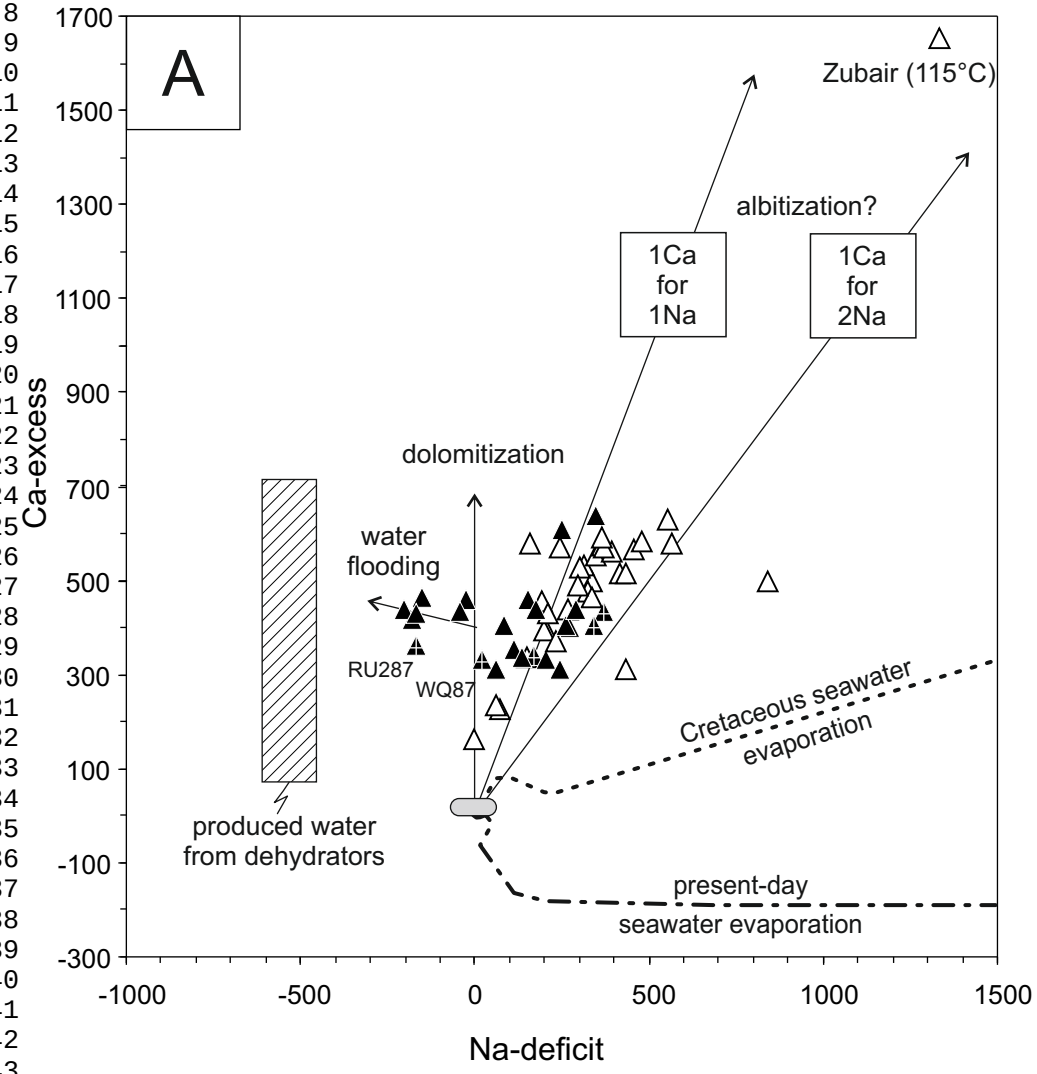
A
Zubair (115°C)
albitization?
1Ca
for
1Na
1Ca
for
2Na
dolomitization
water
flooding
RU287
WQ87
Cretaceous seawater
evaporation
produced water
from dehydrators
present-day
seawater evaporation
Ca-excess
Na-deficit
1700
1500
1300
1100
900
700
500
300
100
-100
-300
-1000
-500
0
500
1000
1500

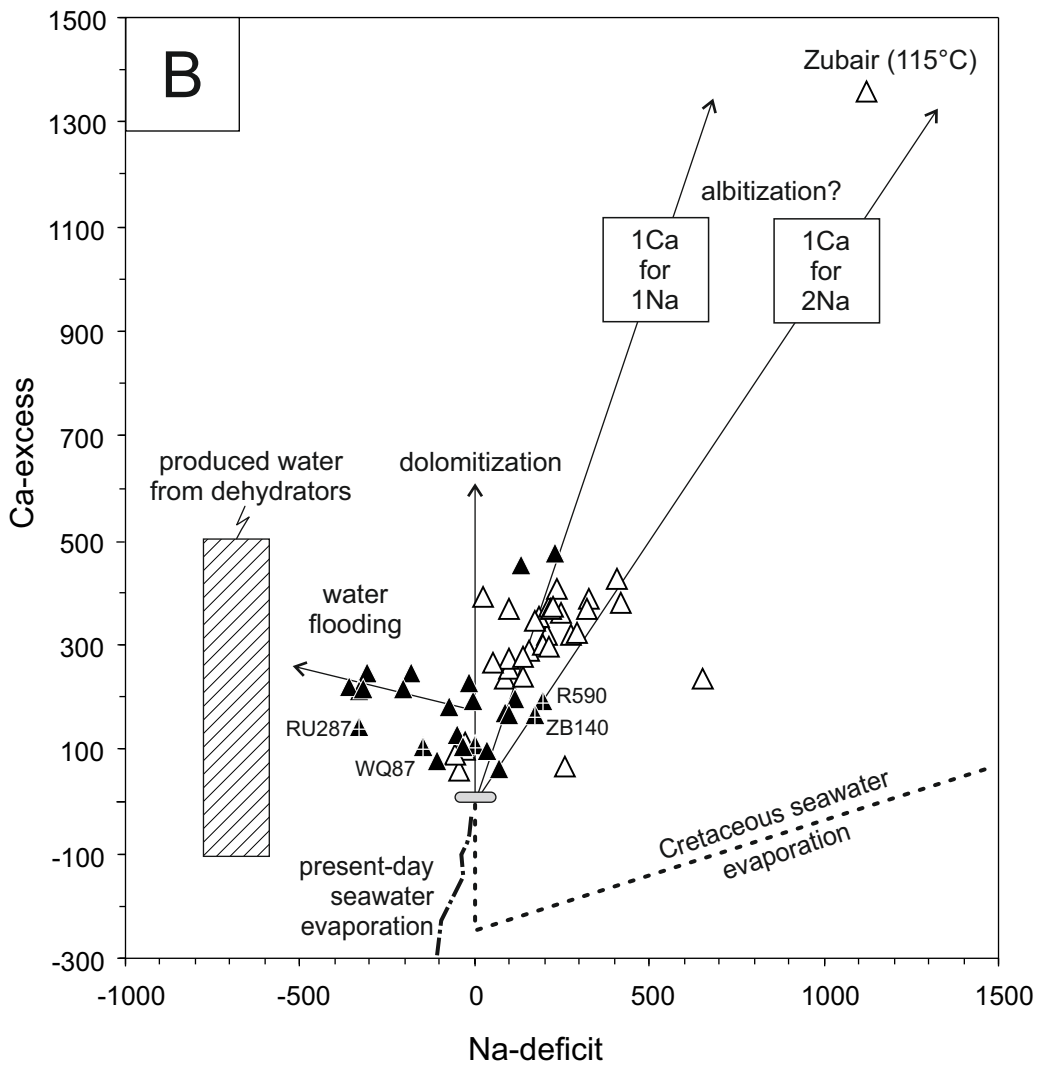
B
Zubair (115°C)
albitization?
1Ca
for
1Na
1Ca
for
2Na
produced water
from dehydrators
dolomitization
water
flooding
RU287
WQ87
R590
ZB140
present-day
seawater
evaporation
Cretaceous seawater
evaporation
Ca-excess
Na-deficit
1500
1300
1100
900
700
500
300
100
-100
-300
-1000
-500
0
500
1000
1500

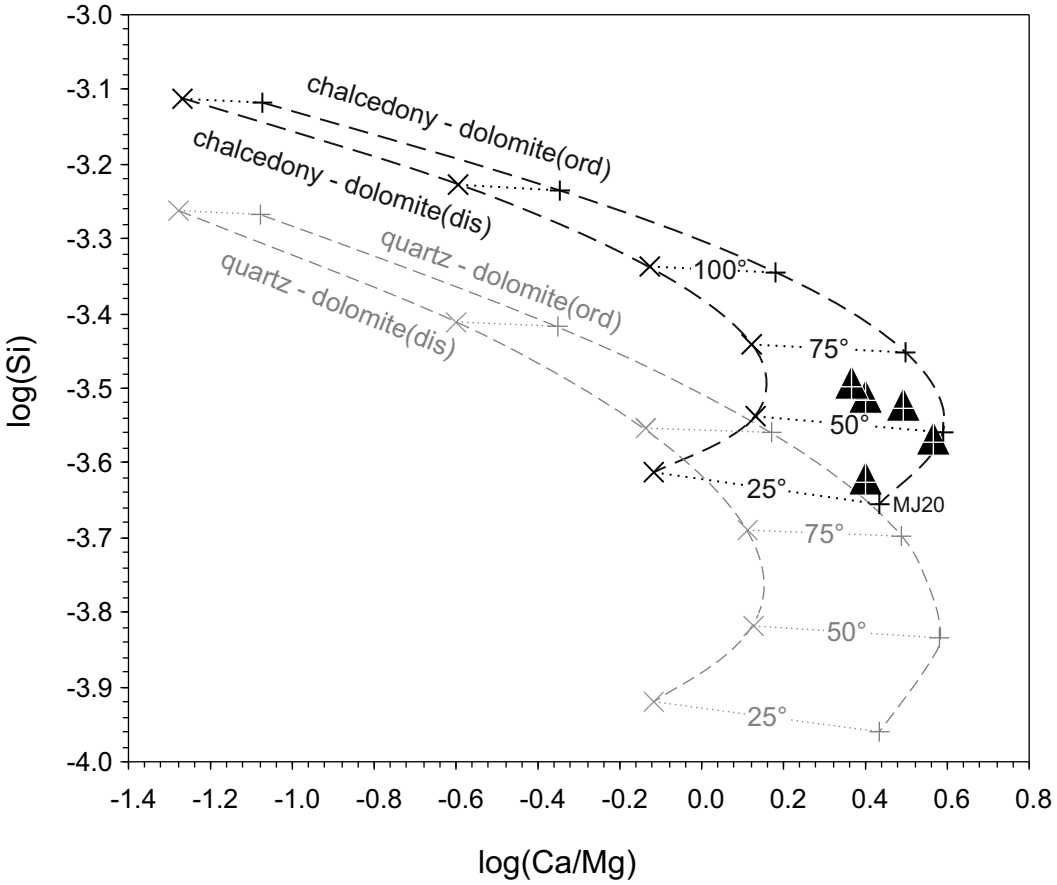
chalcedony - dolomite(ord)
chalcedony - dolomite(dis)
quartz - dolomite(ord)
quartz - dolomite(dis)
100°
75°
50°
25°
MJ20
75°
50°
25°
log(Si)
log(Ca/Mg)
-3.0
-3.1
-3.2
-3.3
-3.4
-3.5
-3.6
-3.7
-3.8
-3.9
-4.0
-1.4
-1.2
-1.0
-0.8
-0.6
-0.4
-0.2
0.0
0.2
0.4
0.6
0.8

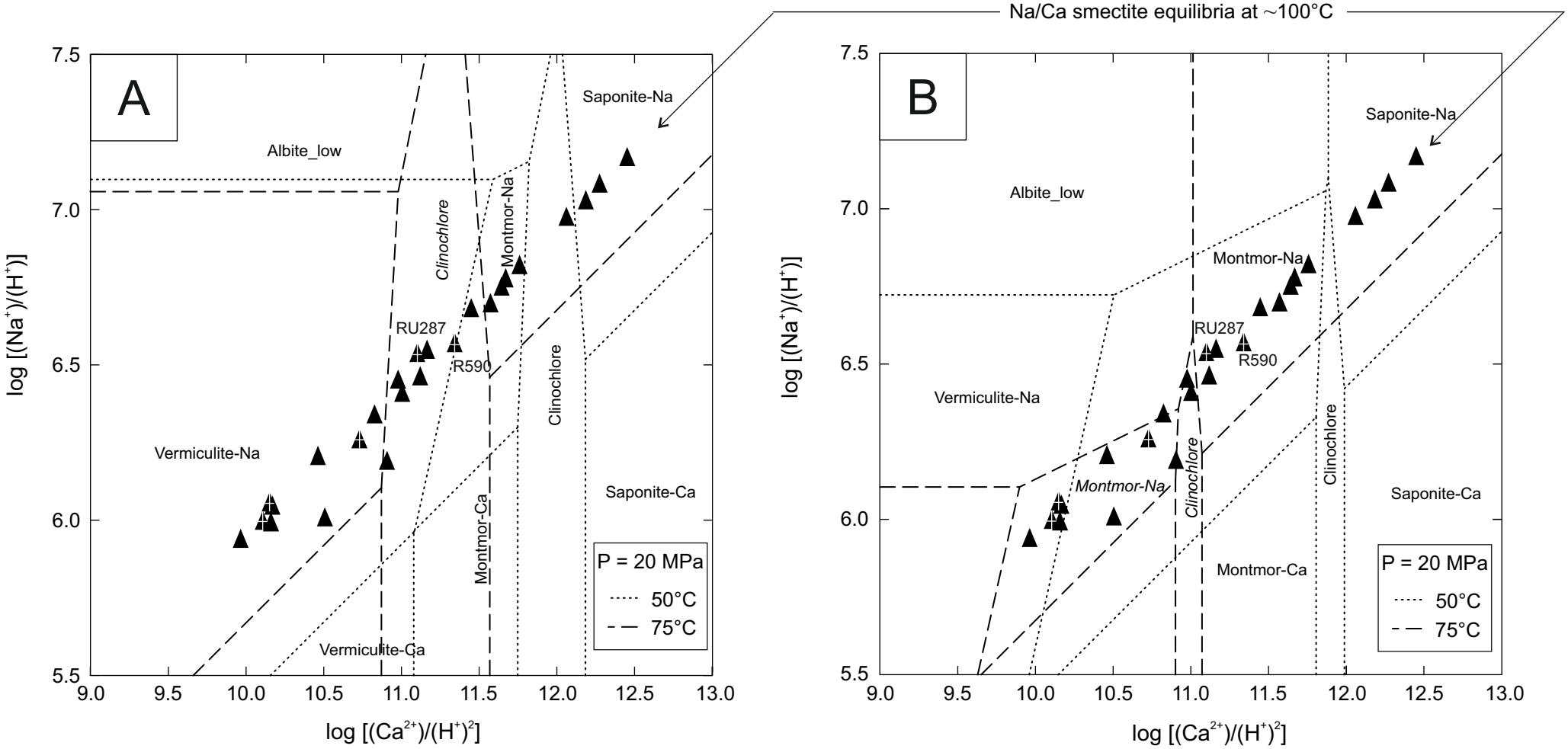
Na/Ca smectite equilibria at ~100°C
A
B
Albite_low
Saponite-Na
Saponite-Ca
Vermiculite-Na
Vermiculite-Ca
Montmor-Na
Montmor-Ca
Clinochlore
RU287
R590
P = 20 MPa
50°C
75°C
log [(Na+)/(H+)]
log [(Ca2+)/(H+)2]
7.5
7.0
6.5
6.0
5.5
9.0
9.5
10.0
10.5
11.0
11.5
12.0
12.5
13.0

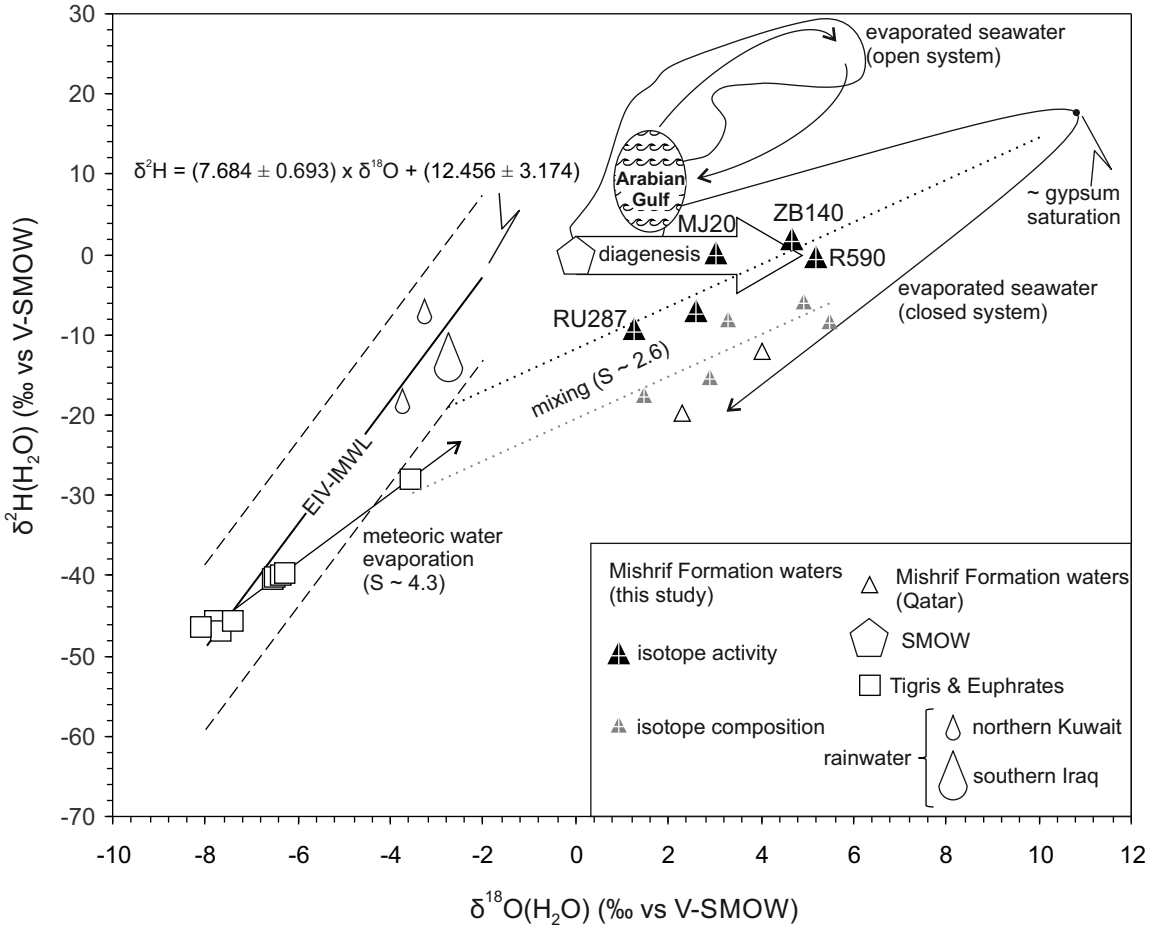
δ²H = (7.684 ± 0.693) x δ¹⁸O + (12.456 ± 3.174)
evaporated seawater (open system)
Arabian Gulf
MJ20
ZB140
R590
diagenesis
~ gypsum saturation
evaporated seawater (closed system)
RU287
mixing (S ~ 2.6)
EIV-IMWL
meteoric water evaporation (S ~ 4.3)
Mishrif Formation waters (this study)
Mishrif Formation waters (Qatar)
isotope activity
SMOW
Tigris & Euphrates
isotope composition
rainwater
northern Kuwait
southern Iraq
δ²H(H₂O) (‰ vs V-SMOW)
δ¹⁸O(H₂O) (‰ vs V-SMOW)
30
20
10
0
-10
-20
-30
-40
-50
-60
-70
-10
-8
-6
-4
-2
0
2
4
6
8
10
12

Table

Table 1

borehole code	unit	RU287	R590	WQ87	MJ20	*ZB140	mean	±	std.dev.	CV %	N	reference
depth oil	m	2438	2682	2295	2836	2464	2412	±	118	5	28	Awadh et al. 2018
depth water	m	2700	2362	2316	2646	2377	2588	±	151	6	28	Awadh et al. 2018
oil pressure	kPa	29027	27717	25511	28613	27614	26977	±	1139	4	28	Awadh et al. 2018
water pressure	kPa	28751	30337	24759	32095	28269	28185	±	2292	8	28	Awadh et al. 2018
Temperature	°C	66	65	67	60	64	65	±	2	3	28	Awadh et al. 2018
pH		6.0	6.1	5.5	5.5	5.8	6.0	±	0.4	6	28	Awadh et al. 2018
Eh (S^{-II}/S^{VI} redox couple)	V	-	-0.165	-0.118	-0.120	-0.140	-0.144	±	0.023	-16	8	this study
TDS	mg/l	235500	255997	248000	249123	246798	243342.75	±	21229	9	28	Awadh et al. 2018
Na	mg/l	83500	77987	82413	80945	77994	78508	±	8561	11	28	Awadh et al. 2018
Ca	mg/l	10300	11980	9870	10105	11356	11417	±	1351	12	28	Awadh et al. 2018
Mg	mg/l	2000	2895	2587	2445	1880	2391	±	543	23	28	Awadh et al. 2018
K	mg/l	1750	2740	1800	2290	480	1709	±	767	45	28	Awadh et al. 2018
Cl	mg/l	143000	155341	148900	152410	154260	145857	±	14281	10	28	Awadh et al. 2018
SO_4	mg/l	1000	360	550	213	385	595	±	347	58	28	Awadh et al. 2018
HCO_3	mg/l	200	120	162	416	196	208	±	89	43	28	Awadh et al. 2018
sulfide as S	mg/l	-	144	68	64	86	103	±	38	37	8	this study
Li	mg/l	4.20	4.06	3.88	5.28	3.09	4.35	±	0.90	21	9	this study
Ba	mg/l	1.77	1.79	1.71	5.43	1.44	2.28	±	1.73	76	9	this study
Sr	mg/l	392	384	365	330	299	371	±	47	13	9	this study
Rb	mg/l	0.80	0.90	0.80	0.80	0.80	0.86	±	0.09	10	9	this study
Fe	mg/l	0.20	0.25	0.22	0.25	0.18	0.25	±	0.04	16	9	this study
Mn	mg/l	0.12	0.12	0.13	4.47	0.10	0.82	±	1.52	184	9	this study
SiO_2	mg/l	15.5	17.0	16.5	13.0	15.0	15.4	±	1.6	10	5	this study
B	mg/l	31.1	28.1	30.8	21.9	*24.9*	27.4	±	3.9	14	5	Awadh et al. 2018
$\delta^{11}B$	‰	35.8	35.9	35.8	33.7	*35.6*	35.4	±	0.9	3	5	Awadh et al. 2018
$\delta^{18}O(H_2O)c$	‰	1.47	5.48	2.89	3.30	4.94	3.6	±	1.6	45	5	this study
$\delta^{2}H(H_2O)c$	‰	-17.4	-8.4	-15.3	-8.1	-5.8	-11.0	±	5.0	-46	5	this study
$10^3 ln\Gamma(^{18}O)$	‰	-0.23	-0.29	-0.31	-0.26	-0.26	-0.27	±	0.03	-11	5	this study

$10^3 \ln\Gamma(^2H)$	‰	8.0	8.0	8.3	8.3	7.8	8.1	±	0.2	3	5	this study
$\delta^{18}O(H_2O)a$	‰	1.24	5.19	2.58	3.04	4.68	3.35	±	1.60	48	5	this study
$\delta^{2}H(H_2O)a$	‰	-9.40	-0.42	-6.99	0.18	1.93	-2.94	±	4.95	-168	5	this study
$^{87}Sr/^{86}Sr$		0.707729	0.707749	0.707724	0.708043	0.707713	0.707792	±	0.000141	0.02	5	this study

* boron concentration and stable isotope ratio from ZB142 borehole (*in italic*).

\- not measured or not detected.

Table 2

	RU287	R590	WQ87	MJ20	ZB140	mean	±	std.dev.	CV %	N	
	geothermometers [°C]										reference
Li-Mg	65	61	61	68	59	64	±	5	8	9	Kharaka and Mariner 1989 (equation 19 in that work)
Li-Mg	64	59	59	68	57	63	±	6	9	9	Kharaka and Mariner 1989 (equation 18 in that work)
*Quartz	97	97	101	86	89	94	±	6	7	5	Kharaka and Mariner 1989 (table 6.4, equation 1 in that work)
*Chalcedony	67	66	71	55	58	64	±	7	10	5	Kharaka and Mariner 1989 (table 6.4, equation 2 in that work)
Na-Li	40	41	38	47	34	42	±	6	13	9	Kharaka and Mariner 1989 (table 6.4, equation 8 in that work)
Na-Li	40	41	39	48	34	42	±	6	13	9	Sanjuan et al. 2014 (equation 9 in that work)
$\delta^{11}B$	19	18	19	32	20	21	±	6	27	5	Boschetti et al. 2015
†$\delta^{11}B$-corrected	61	61	61	74	61	64	±	6	9	5	Boschetti et a. 2015; this work
B	73	70	72	62	66	68	±	5	7	5	Boschetti et al. 2016 (equation 3 in that work)
♠mean	66	63	65	68	60						
♠std.dev.	4	4	6	4	3						
	saturation indexes [SI = (logIAP)/(logK)]										code
calcite	1.1	1.0	0.58	0.87	0.92	1.1	±	0.4	34	28	PHREEQCI
aragonite	0.77	0.69	0.24	0.54	0.59	0.78	±	0.38	48	28	PHREEQCI
magnesite	-0.13	-0.27	-0.56	-0.40	-0.44	-0.18	±	0.33	-179	28	PHREEQCI
rhodochrosite	-4.04	-4.31	-4.60	-2.70	-4.31	-3.9	±	0.8	-22	9	PHREEQCI
siderite	-3.16	-3.44	-3.80	-3.40	-3.51	-3.4	±	0.3	-10	9	PHREEQCI
strontianite	-1.19	-1.49	-1.78	-1.55	-1.55	-1.4	±	0.4	-25	9	PHREEQCI
♣carbonates-SS	0.22	0.11	-0.44	-0.21	-0.089	-0.082	±	0.261	-319	5	EQ3/6
dolomite-disordered	1.5	1.4	0.55	1.1	1.0	1.5	±	0.8	52	28	PHREEQCI
dolomite-ordered	1.9	1.8	0.95	1.5	1.4	1.9	±	0.8	41	28	PHREEQCI
quartz	0.30	0.30	0.33	0.25	0.24	0.28	±	0.03	12	5	PHREEQCI
chalcedony	-0.024	-0.021	0.0088	-0.080	-0.082	-0.040	±	0.040	-100	5	PHREEQCI
anhydrite	0.094	-0.36	-0.13	-0.65	-0.33	-0.21	±	0.28	-134	28	PHREEQCI
gypsum	-0.15	-0.58	-0.39	-0.82	-0.54	-0.43	±	0.27	-63	28	PHREEQCI
barite	0.061	-0.42	-0.21	-0.061	-0.43	-0.45	±	0.58	-129	9	PHREEQCI
halite	-0.44	-0.50	-0.41	-0.47	-0.53	-0.50	±	0.15	-31	28	PHREEQCI
log$P(CO_2)g$	-0.45	-0.77	-0.050	0.352	-0.25	-0.46	±	0.41	-91	28	PHREEQCI

* the equation takes into account the effects of pressure and salinity on mineral solubility;

† before calculation, both the effect due to Cretaceous seawater (-3‰) and evaporation (-4‰) were subtracted from the values of the brine samples (Table 1);

♠ all geothermometric results were considered, except those from Na-Li equations and uncorrected $\delta^{11}B$. For MJ20, the standard deviation was calculated considering the central value of the temperature obtained by quartz and calcedony equation (see Fig. 4 and text for details).

♣ calcite, magnesite, siderite, strontianite and rhodocrosite solid solution.

Supplementary Material (for online publication only)

Click here to download Supplementary Material (for online publication only): Supplementary File 1.docx

***Credit Author Statement**

Author Contributions: Conceptualization, TB, SMA and ZMY; Data curation, SMA and TB; Formal analysis, TB, SMA, HSA, PI, LT, ES and ZMY; Investigation, TB, SMA, HSA, PI, LT, ES and ZMY; Methodology, TB and SMA; Project administration, TB, SMA, and ZMY; Resources, SMA; Supervision, TB and SMA; Validation, TB, SMA, HSA, PI, LT, ES and ZM; Visualization, TB, SMA, HSA, PI, LT, ES and ZMY; Writing – original draft, TB, SMA, HSA, PI, LT, ES and ZMY; Writing– review & editing, TB, SMA and ZMY.

*Declaration of Interest Statement

Declaration of interests

☒ The authors declare that they have no known competing financial interests or personal relationships that could have appeared to influence the work reported in this paper.

☐The authors declare the following financial interests/personal relationships which may be considered as potential competing interests:

On behalf of the co-authors

Zaher Mundher Yaseen

Faculty of Civil Engineering,
Ton Duc Thang University,
Ho Chi Minh City,
Vietnam
yaseen@tdtu.edu.vn